

A single-mode quantum transport in serial-structure geometric scatterers

P. Exner,^{1,2} M. Tater,¹ and D. Vaněk³

15/9/2000

*1 Nuclear Physics Institute, Academy of Sciences, CZ-25068 Řež near Prague,
2 Doppler Institute, Czech Technical University, Břehová 7, CZ-11519 Prague,
3 Department of Mathematics, FNSPE, Czech Technical University,
Trojanova 13, CZ-12000 Prague, Czech Republic
exner@ujf.cas.cz, tater@ujf.cas.cz, vanekd@Alenka.ufa.cas.cz*

Abstract

We study transport in quantum systems consisting of a finite array of N identical single-channel scatterers. A general expression of the S matrix in terms of the individual-element data obtained recently for potential scattering is rederived in this wider context. It shows in particular how the band spectrum of the infinite periodic system arises in the limit $N \rightarrow \infty$. We illustrate the result on two kinds of examples. The first are serial graphs obtained by chaining loops or T-junctions. A detailed discussion is presented for a finite-periodic “comb”; we show how the resonance poles can be computed within the Krein formula approach. Another example concerns geometric scatterers where the individual element consists of a surface with a pair of leads; we show that apart of the resonances coming from the decoupled-surface eigenvalues such scatterers exhibit the high-energy behavior typical for the δ' interaction for the physically interesting couplings.

Contents

1	Introduction	2
2	Serial structure transport	3
2.1	Preliminaries	3
2.2	Recursive relations for scattering amplitudes	6
2.3	The S-matrix expression	7
2.4	Relation to band spectra of periodic systems	9

3	Serial graphs	10
3.1	Loop arrays	11
3.2	Band spectrum of an infinite loop array	12
3.3	Comb graphs	13
3.4	Scattering on a comb graph	15
3.5	The resolvent poles	16
3.6	Band spectrum of an infinite comb and resonances	19
4	Serial structures of mixed dimensionality	20
4.1	Coupling of leads to a surface	21
4.2	The single-element S-matrix	22
4.3	A “bubble” on the line	24
4.4	A “bubble” array	30
A	A direct derivation of the comb-graph S-matrix	31

1 Introduction

A rapid progress in experimental solid state physics has expanded dramatically the list of situations in which consequences of the basic equations of quantum mechanics may be tested, since the interaction is prescribed by the experimentalist by the shape design of the structure in question, material choice, *etc.* One of the frequently occurring cases in mesoscopic transport involves a passage of a quantum particle through a *serial* — or finitely periodic — structure obtained by arraying a certain number N of identical scatterers.

Our aim in the present paper is to study this situation under the assumption that the individual scatterers have a single transport mode. For a collection of mesoscopic elements connected by quantum wires, this is certainly an idealization. We can adopt this approximation provided the transverse modes in the wires are well separated and the distances between the scatterers are large enough so that the intermode coupling and influence of the evanescent modes can be neglected.

Such a single-mode transport is often investigated in literature, with the S-matrix obtained either “inductively” by adding the scatterers successively or by means of the transfer matrix method. It is difficult to collect all relevant references but a representative sample is given in [26]; an extension of this “factorization” method to scattering on graphs was proposed recently in [35]. On the other hand, the mentioned methods are typically used to evaluate the S-matrix numerically and give little insight, say, into its dependence on the number N of the scatterers. To this purpose a transparent expression for the S-matrix is needed.

Such closed-form formulas were derived recently in one-dimensional potential scattering, first for an array of δ interactions [11, 12, 29] and then for an arbitrary finitely periodic potential [39, 45]; also the number of bound states has been discussed in this setting [4, 41]. When this work was in its final stage, another analysis

of this situation appeared [11] which investigated in detail the distribution of scattering resonances and the corresponding time delay. Our basic observation is that the input for the S-matrix expression are the individual-element scattering data, and thus the result can be applied to scattering on an array of arbitrary “black boxes”. In the next section we rederive the result of [39, 45] in this more general context.

We apply the whole scheme to two models of quantum particles confined to a graph in Sec. 3. The first model consists of an array of planar loops joined by a pair of external leads. The system is placed into a homogeneous magnetic field perpendicular to the graph plane. From several ways how to couple quantum motion on a branching graph in a self-adjoint way we investigate only δ coupling. The next model discussed in this section is made of identical appendices attached to a line, called comb-shaped graph. The motion on the line is free, however the particle can interact with an external (scalar) potential on appendices. We study the most general self-adjoint way of coupling with the wave function continuous on the line, the only limitation comes from time-reversal invariance. It leads to a three-parametric family of solutions. Dependence of transmission probability and resolvent poles on the number of appendices and the coupling parameters is analyzed and band spectrum of an infinite comb is discussed as well.

A step more complicated situation is investigated in section 4; scatterers with dimension two are coupled to single-mode leads. First, we impose suitable boundary conditions at the junction ensuring self-adjointness and show their relevancy to the experimentally observed data. Then we specify our formalism to spheres and find explicit expressions for the transmission coefficient. We prove existence of resonance peaks and the background which dominates at large energies and decays not slower than E^{-1} as $E \rightarrow \infty$. Furthermore, we conjecture that the “coarse grained” transmission probability (averaged locally over the resonances) has the E^{-1} decay typical for the δ' interaction. Finally, we present band spectrum of infinite system.

2 Serial structure transport

2.1 Preliminaries

Consider an equidistant array $\{\mathcal{S}_j : j = 0, \dots, N-1\}$ of identical scatterers placed at the line points $x_0 + j\ell$. The spacing $\ell \geq 0$ in this convention includes only the distance between \mathcal{S}_j and \mathcal{S}_{j+1} , not the possible size of the scatterers themselves.

Let us review briefly basic notions concerning a single-mode scattering on a sole scatterer \mathcal{S} placed conventionally at the point $x_0 = 0$. On the two halflines attached to \mathcal{S} the particle moves as free, so the on-shell S-matrix at energy k^2 ,

$$\begin{pmatrix} B_+ \\ B_- \end{pmatrix} = S \begin{pmatrix} A_+ \\ A_- \end{pmatrix}, \quad (2.1)$$

couples the coefficients of the asymptotic solutions

$$\psi(x) = \begin{cases} A_+ e^{ikx} + B_- e^{-ikx} & \dots & x < 0 \\ B_+ e^{ikx} + A_- e^{-ikx} & \dots & x > 0 \end{cases} \quad (2.2)$$

In particular, we have

$$S = \begin{pmatrix} t & \tilde{r} \\ r & \tilde{t} \end{pmatrix}, \quad (2.3)$$

where r, t and \tilde{r}, \tilde{t} are the left-to-right and right-to-left reflection and transmission amplitudes, respectively. We shall consider only the non-dissipative situation when S is unitary; its dependence on the momentum k will be indicated only if necessary.

Since the interaction responsible for the scattering is localized by assumption, solutions to the Schrödinger equation acquire the asymptotic form outside the scatterer. Hence S may be expressed alternatively in terms matrices used in the theory of ordinary differential equations. One is the ‘‘coefficient’’ transfer matrix M relating the solutions to the left and to the right of the scatterer by

$$\begin{pmatrix} B_+ \\ A_- \end{pmatrix} = M \begin{pmatrix} A_+ \\ B_- \end{pmatrix}. \quad (2.4)$$

It is straightforward to see that

$$M = \frac{1}{\tilde{t}} \begin{pmatrix} t\tilde{t} - r\tilde{r} & \tilde{r} \\ -r & 1 \end{pmatrix}, \quad (2.5)$$

and vice versa,

$$r = -\frac{M_{21}}{M_{22}}, \quad t = M_{11} - \frac{M_{12}M_{21}}{M_{22}}, \quad \tilde{r} = \frac{M_{12}}{M_{22}}, \quad \tilde{t} = \frac{1}{M_{22}}. \quad (2.6)$$

Another one is the transfer matrix which relates the values and derivatives of the two solutions,

$$\begin{pmatrix} u(0+) \\ u'(0+) \end{pmatrix} = L \begin{pmatrix} u(0-) \\ u'(0-) \end{pmatrix}. \quad (2.7)$$

Substituting the boundary values of $u(x) = e^{ikx} + r e^{-ikx}$ for $x < 0$ and $u(x) = t e^{ikx}$ for $x > 0$ into this relation, we get a pair of equations for r, t which is solved by

$$r = -\frac{L_{21} + ik(L_{22} - L_{11}) + k^2 L_{12}}{L_{21} - ik(L_{22} + L_{11}) - k^2 L_{12}}, \quad (2.8)$$

$$t = -\frac{2ik \det L}{L_{21} - ik(L_{22} + L_{11}) - k^2 L_{12}}$$

In the same way we get the right-to-left amplitudes,

$$\tilde{r} = -\frac{L_{21} + ik(L_{11} - L_{22}) + k^2 L_{12}}{L_{21} - ik(L_{22} + L_{11}) - k^2 L_{12}}, \quad (2.9)$$

$$\tilde{t} = -\frac{2ik}{L_{21} - ik(L_{22} + L_{11}) - k^2 L_{12}}$$

Combining (2.5) with (2.8), (2.9) we can express the ‘‘coefficient’’ transfer matrix as

$$M = \frac{1}{2ik} \begin{pmatrix} L_{21} + ik(L_{11} + L_{22}) - k^2 L_{12} & L_{21} + ik(L_{11} - L_{22}) + k^2 L_{12} \\ -L_{21} + ik(L_{11} - L_{22}) - k^2 L_{12} & -L_{21} + ik(L_{11} + L_{22}) + k^2 L_{12} \end{pmatrix}. \quad (2.10)$$

The class of admissible transfer matrices is restricted by the S–matrix unitarity. In particular, the conservation of probability current, $|r|^2 + |t|^2 = |\tilde{r}|^2 + |\tilde{t}|^2 = 1$ implies $|\det L| = 1$; we shall write therefore

$$\det L = \frac{t}{\tilde{t}} =: e^{2i\varphi}. \quad (2.11)$$

One can also express L by means of the other two matrices. For instance, suppose that (2.3) is given. Using the relation (2.7) with the boundary values for the left–to–right scattering, the same for the right–to–left case with the explicitly written L^{-1} and $t = \tilde{t} \det L$, we get a system of four linear equations for L_{jk} ,

$$L_{11}(1+r) + ikL_{12}(1-r) = t, \quad L_{21}(1+r) + ikL_{22}(1-r) = ikt, \quad (2.12)$$

$$L_{22}(1+\tilde{r}) + ikL_{12}(1-\tilde{r}) = t, \quad L_{21}(1+\tilde{r}) + ikL_{11}(1-\tilde{r}) = ikt.$$

Only three of them are independent; it is straightforward to see that the first with the third, and the second with the fourth equation lead to the same relation which is solved by

$$L_{22} = L_{11} \frac{(1+r)(1-\tilde{r})}{(1-r)(1+\tilde{r})} - \frac{t(r-\tilde{r})}{(1-r)(1+\tilde{r})}.$$

The same pairs of equations allow us to express L_{12} and L_{21} in terms of L_{11} and L_{22} ; in combination with the last relation we find

$$L_{12} = -L_{11} \frac{(1+r)}{ik(1-r)} + \frac{t}{ik(1+\tilde{r})}, \quad L_{21} = -ikL_{11} \frac{(1-\tilde{r})}{ik(1+\tilde{r})} + \frac{ikt}{(1+\tilde{r})}.$$

We have still the condition (2.11). Computing the determinant with the help of the above relations, we get

$$\det L = \frac{t(2L_{11} - t)}{(1-r)(1+\tilde{r})} = \frac{t}{\tilde{t}}.$$

One can express L_{11} from here and substitute into the formulas for the other elements; this yields finally

$$L = \frac{1}{2\tilde{t}} \begin{pmatrix} t\tilde{t} + (1+r)(1-\tilde{r}) & \frac{1}{ik} [t\tilde{t} - (1+r)(1+\tilde{r})] \\ ik [t\tilde{t} - (1-r)(1-\tilde{r})] & t\tilde{t} + (1-r)(1+\tilde{r}) \end{pmatrix}. \quad (2.13)$$

The determinant of this matrix is equal to the middle expression of (2.11) and substituting into (2.8), (2.9) one can check that (2.13) indeed represents the inverse transformation.

Furthermore, the unitarity of S has a stronger consequence. It is well known that a general 2×2 unitary matrix can be parametrized by four real numbers as

$$e^{i\xi} \begin{pmatrix} e^{i(\alpha+\delta)} \cos \beta & e^{i(\delta-\alpha)} \sin \beta \\ -e^{i(\alpha-\delta)} \sin \beta & e^{-i(\alpha+\delta)} \cos \beta \end{pmatrix}.$$

Using this for S given by (2.3) and substituting into (2.13) we find that

$$L = e^{i\varphi} \mathcal{L}, \quad \mathcal{L} \text{ real with } \det \mathcal{L} = 1, \quad (2.14)$$

where $\varphi := \alpha + \delta$. Notice that M given by (2.10) has then the following property:

$$\overline{M}_{11} = e^{-2i\varphi} M_{22}, \quad \overline{M}_{12} = e^{-2i\varphi} M_{21}. \quad (2.15)$$

2.2 Recursive relations for scattering amplitudes

Before we derive the mentioned closed-form expression, let us recall the usual factorization technique. We index the transmission and reflection amplitudes for the array by N . In analogy with (2.3) we have

$$\begin{pmatrix} B_-^N \\ B_+^N \end{pmatrix} = \begin{pmatrix} r_N & \tilde{t}_N \\ t_N & \tilde{\varepsilon}^{2(N-1)} \tilde{r}_N \end{pmatrix} \begin{pmatrix} A_+^N \\ A_-^N \end{pmatrix}, \quad (2.16)$$

where $\varepsilon := e^{ik\ell}$. Next we add the $(N+1)$ -th scatterer to the right side of the array for which

$$\begin{pmatrix} B_- \\ B_+ \end{pmatrix} = \begin{pmatrix} \varepsilon^{2N} r & \tilde{t} \\ t & \tilde{\varepsilon}^{2N} \tilde{r} \end{pmatrix} \begin{pmatrix} A_+ \\ A_- \end{pmatrix}, \quad (2.17)$$

where, of course, $B_+^N = A_+$ and $B_- = A_-^N$. In analogy with (2.5) we rewrite the last two relations in the ‘‘coefficient’’ transfer matrix form. Multiplying the two matrices we get $\begin{pmatrix} B_+ \\ A_- \end{pmatrix} = M \begin{pmatrix} A_+^N \\ B_-^N \end{pmatrix}$ with

$$M := \begin{pmatrix} \frac{1}{\tilde{t}\tilde{t}_N} ((\tilde{t}\tilde{t} - r\tilde{r})(t_N \tilde{t}_N - r_N \tilde{r}_N \tilde{\varepsilon}^{2(N-1)}) - r_N \tilde{r} \tilde{\varepsilon}^{2N}) & \frac{1}{\tilde{t}\tilde{t}_N} ((\tilde{t}\tilde{t} - r\tilde{r}) \tilde{r}_N + \tilde{\varepsilon}^{2N} \tilde{r}) \\ \frac{1}{\tilde{t}\tilde{t}_N} (-\varepsilon^{2N} r (t_N \tilde{t}_N - r_N \tilde{r}_N) - r_N) & \frac{1}{\tilde{t}\tilde{t}_N} (1 - \varepsilon^{2N} r \tilde{r}_N) \end{pmatrix}.$$

Comparing this with (2.6) we find the sought recursive relations

$$\tilde{r}_{N+1} = \tilde{\varepsilon}^{2N} \tilde{r} + \frac{\tilde{r}_N \tilde{t}\tilde{t}}{1 - \varepsilon^{2N} \tilde{r}_N r}, \quad \tilde{t}_{N+1} = \frac{\tilde{t}\tilde{t}_N}{1 - \varepsilon^{2N} r \tilde{r}_N}. \quad (2.18)$$

If we modify the argument by adding the $(N+1)$ -th scatterer to the left of the array, we get in the same way

$$r_{N+1} = \varepsilon^{2N} r + \frac{r_N \tilde{t}\tilde{t}}{1 - \tilde{\varepsilon}^{2N} \tilde{r}_N r}, \quad t_{N+1} = \frac{t\tilde{t}_N}{1 - \tilde{\varepsilon}^{2N} r_N \tilde{r}}. \quad (2.19)$$

Since the ‘‘component’’ S-matrices are unitary, it is straightforward to check by induction that the same is true for the total S-matrix. The relations (2.18) and (2.19) have a transparent meaning: expanding the fractions into geometric series we obtain expressions containing sums of contributions from various scattering processes.

2.3 The S–matrix expression

On the other hand, the recursive expressions do not relate directly the S–matrices of an individual scatterer and that of the whole array. To this end, notice first that in view of (2.15) we can write the M matrix of the j –th scatterer as

$$M_j = e^{i\varphi} \begin{pmatrix} \bar{R} & \bar{\varepsilon}^{2j}\bar{S} \\ \varepsilon^{2j}S & R \end{pmatrix}, \quad (2.20)$$

where $\varepsilon := e^{ik\ell}$ as above and

$$R := e^{-i\varphi} M_{22} = \frac{e^{-i\varphi}}{\tilde{t}} = \frac{e^{i\varphi}}{t} = \frac{\mathcal{L}_{11} + \mathcal{L}_{22}}{2} + i \left(\frac{\mathcal{L}_{21}}{2k} - \frac{k}{2} \mathcal{L}_{12} \right), \quad (2.21)$$

$$S := e^{-i\varphi} M_{21} = -\frac{e^{-i\varphi} r}{\tilde{t}} =: -\frac{e^{i\varphi} r}{t} = \frac{\mathcal{L}_{11} - \mathcal{L}_{22}}{2} + i \left(\frac{\mathcal{L}_{21}}{2k} + \frac{k}{2} \mathcal{L}_{12} \right).$$

By definition the “coefficient” transfer matrix of the array is obtained by multiplying successively the matrices (2.20). We denote $M^{(n)} := M_n M_{n-1} \dots M_0$. It is easy to compute the first few matrices $M^{(n)}$; this inspires us to look for the general product in the form

$$M^{(n)} = e^{i(n+1)\varphi} \begin{pmatrix} \bar{\varepsilon}^{n+1}|S|^{n+1}\bar{\gamma}_n & \bar{\varepsilon}^n \bar{S} |S|^n \bar{\delta}_n \\ \varepsilon^n S |S|^n \delta_n & \varepsilon^{n+1} |S|^{n+1} \gamma_n \end{pmatrix}, \quad (2.22)$$

where the coefficients have to satisfy the recursive relations

$$\gamma_{n+1} = \zeta \gamma_n + \bar{\delta}_n, \quad \delta_{n+1} = \zeta \delta_n + \bar{\gamma}_n \quad (2.23)$$

with $\delta_0 = 1$ and

$$\gamma_0 = \zeta := \frac{\bar{\varepsilon} R}{|S|}, \quad (2.24)$$

which follows from $M^{(n+1)} = M_{n+1} M^{(n)}$. Since

$$\det M_j = e^{2i\varphi} (|R|^2 - |S|^2) = e^{2i\varphi} \frac{1 - |r|^2}{|\tilde{t}|^2} = e^{2i\varphi}, \quad (2.25)$$

and consequently, $\det M^{(n)} = e^{2i(n+1)\varphi} |S|^{2n+2} (|\gamma_n|^2 - |\delta_n|^2) = e^{2i(n+1)\varphi}$, we have

$$\gamma_n = e^{i\theta_n} \sqrt{|\delta_n|^2 + |S|^{-2n-2}} \quad (2.26)$$

with a phase factor to be determined. Substituting into the relations (2.23) we get

$$e^{i\theta_{n+1}} \sqrt{|\delta_{n+1}|^2 + |S|^{-2n-4}} = \zeta e^{i\theta_n} \sqrt{|\delta_n|^2 + |S|^{-2n-2}} + \delta_n, \quad (2.27)$$

$$\delta_{n+1} = \zeta \delta_n + e^{-i\theta_n} \sqrt{|\delta_n|^2 + |S|^{-2n-2}}.$$

We express $e^{i\theta_n}$ from the second equation and substitute into the first one; this yields

$$\delta_{n+2} - (\zeta + \bar{\zeta})\delta_{n+1} + (|\zeta|^2 - 1)\delta_n = 0. \quad (2.28)$$

Now $\delta_0 = 1$ and $\delta_1 = \zeta + \bar{\zeta}$, so (2.28) is solved by

$$\delta_n = (|\zeta|^2 - 1)^{n/2} U_n \left(\frac{\zeta + \bar{\zeta}}{2\sqrt{|\zeta|^2 - 1}} \right),$$

where U_n is the Chebyshev polynomial of the second kind. Since $|\zeta|^2 - 1 = |S|^{-2}$ by (2.25), its argument can be more compactly written as $\text{Re}(\bar{\varepsilon}R)$. Using (2.26) and (2.27) again, we find $M^{(n)} = e^{2i(n+1)\varphi} \mathcal{M}^{(n)}$ with

$$\mathcal{M}^{(n)} = \begin{pmatrix} \bar{\varepsilon}^{n+1} e^{-i\theta_n} \sqrt{1 + |S|^2 U_n(\text{Re}(\bar{\varepsilon}R))^2} & \bar{\varepsilon}^n \bar{S} U_n(\text{Re}(\bar{\varepsilon}R)) \\ \varepsilon^n S U_n(\text{Re}(\bar{\varepsilon}R)) & \varepsilon^{n+1} e^{i\theta_n} \sqrt{1 + |S|^2 U_n(\text{Re}(\bar{\varepsilon}R))^2} \end{pmatrix}, \quad (2.29)$$

where

$$e^{i\theta_n} = \frac{U_{n+1}(\text{Re}(\bar{\varepsilon}R)) - \varepsilon \bar{R} U_n(\text{Re}(\bar{\varepsilon}R))}{\sqrt{1 + |S|^2 U_n^2(\text{Re}(\bar{\varepsilon}R))}}. \quad (2.30)$$

Now we may employ (2.5) and (2.11) to find the sought formulas for the array of N scatterers; it is sufficient to put $n = N - 1$. We arrive at the following conclusion:

Theorem 2.1 *With the given notation, the transmission and reflection amplitudes of an N -element serial structure express as*

$$t_N = \frac{\bar{\varepsilon}^N e^{-i\theta_{N-1}}}{\sqrt{1 + |S|^2 U_{N-1}(\text{Re}(\bar{\varepsilon}R))^2}} \quad (2.31)$$

$$r_N = -\frac{\bar{\varepsilon} e^{-i\theta_{N-1}} S U_{N-1}(\text{Re}(\bar{\varepsilon}R))}{\sqrt{1 + |S|^2 U_{N-1}(\text{Re}(\bar{\varepsilon}R))^2}}, \quad (2.32)$$

where the phase factor is given by (2.30). In the same way the right-to-left amplitudes are $\tilde{t}_N = t_N e^{-2iN\varphi}$ and

$$\tilde{r}_N = -\frac{\bar{\varepsilon}^{2N-1} e^{-i\theta_{N-1}} \bar{S} U_{N-1}(\text{Re}(\bar{\varepsilon}R))}{\sqrt{1 + |S|^2 U_{N-1}(\text{Re}(\bar{\varepsilon}R))^2}}.$$

In particular, the transmission and reflection probabilities are the same in both directions and equal

$$|t_N|^2 = \frac{1}{1 + |S|^2 U_{N-1}(\text{Re}(\bar{\varepsilon}R))^2}, \quad |r_N|^2 = \frac{|S|^2 U_{N-1}(\text{Re}(\bar{\varepsilon}R))^2}{1 + |S|^2 U_{N-1}(\text{Re}(\bar{\varepsilon}R))^2}. \quad (2.33)$$

Recall that

$$|S|^2 = \left| \frac{r}{t} \right|^2, \quad \text{Re}(\bar{\varepsilon}R) = \text{Re} \left(\frac{e^{-i(k\ell+\varphi)}}{\tilde{t}} \right) = \text{Re} \left(\frac{e^{-i(k\ell-\varphi)}}{t} \right);$$

it is obvious from (2.33) that the probability current is preserved.

2.4 Relation to band spectra of periodic systems

Consider now an infinite periodic array of identical scatterers \mathcal{S} joined by line segments of length ℓ . The one-period transfer matrix is $T = L\mathcal{U}_\ell(k)$, where

$$\mathcal{U}_\ell(k) := \begin{pmatrix} \cos k\ell & \frac{1}{k} \sin k\ell \\ -k \sin k\ell & \cos k\ell \end{pmatrix}$$

corresponds to the segment. The band spectrum of the problem is given by the Bloch condition, $\det(T - e^{i\theta}) = 0$, or

$$e^{2i\theta} - e^{i\theta} \operatorname{tr} T + \det T = 0. \quad (2.34)$$

In view of (2.11), $\det T = \det L = e^{2i\varphi}$, so the condition may be written as

$$e^{-i\varphi} \operatorname{tr} T = 2 \cos(\theta - \varphi).$$

To express the *lhs*, we employ (2.13) which yields

$$\operatorname{tr} T = \operatorname{tr} T \cos k\ell + \left(\frac{1}{k} L_{21} - k L_{12} \right) \sin k\ell = \frac{t\tilde{t} - r\tilde{r}}{\tilde{t}} e^{ik\ell} + \frac{1}{\tilde{t}} e^{-ik\ell},$$

and since

$$\frac{t\tilde{t} - r\tilde{r}}{\tilde{t}} = \frac{e^{2i\varphi}}{\tilde{t}}$$

by (2.5) and (2.15), we arrive finally at

$$\operatorname{Re}(\bar{\varepsilon}R) = \frac{e^{i(k\ell+\varphi)}}{2\tilde{t}} + \frac{e^{-i(k\ell+\varphi)}}{2\tilde{t}} = \cos(\theta - \varphi). \quad (2.35)$$

The *lhs* as a function of k is typically oscillating. Since the amplitude $|t|^{-1} > 1$ unless the single-element scattering is reflectionless, the periodic spectrum has gaps in general.

The relations (2.33) show how the band spectrum arises in the limit $N \rightarrow \infty$ of the serial-structure scattering. The Chebyshev polynomials

$$U_n(x) = \sum_{m=0}^{\lfloor n/2 \rfloor} (-1)^m \frac{(n-m)!}{m!(n-2m)!} (2x)^{n-2m} \quad (2.36)$$

are oscillating within the interval $[-1, 1]$. The easiest way to see that is to use the representation

$$U_n(x) = \frac{\sin(n+1)\xi}{\sin \xi}, \quad \xi := \arccos x. \quad (2.37)$$

Thus U_{N-1} has $N - 1$ roots in $[-1, 1]$ and each band contains at least $N - 1$ points where $|t_N(k)|^2 = 1$. Possible additional points with this property can come from zeros of the single-element reflection coefficient. Properties of Chebyshev polynomials yield also lower bounds to the envelope of the transmission probability

oscillations. The representation (2.37) implies $|U_n(x)| \leq (1-x^2)^{-1/2}$ for $|x| < 1$, and therefore

$$|t_N(k)|^2 \geq \frac{1 - (\operatorname{Re}(\bar{\varepsilon}R))^2}{1 + |S|^2 - (\operatorname{Re}(\bar{\varepsilon}R))^2} = \frac{|t(k)|^2 - (\operatorname{Re}(\tilde{t}(k)e^{i(k\ell+\varphi)}))^2}{1 - (\operatorname{Re}(\tilde{t}(k)e^{i(k\ell+\varphi)}))^2}. \quad (2.38)$$

If $|t(\cdot)|^2$ is a slowly varying function, the *rhs* reaches its maximum $|t(k)|^2$ in the middle of the band; it is zero at the band edges. However, the transmission can vanish within a band only due to a single-element full reflection. This follows from another upper bound [1], $|U_n(x)| \leq (n+1)$ for $|x| \leq 1$, which yields $|t_N|^2 \geq (1 + N^2|S|^2)^{-1}$ or

$$|t_N(k)|^2 \geq \frac{|t(k)|^2}{1 + (N-1)|r(k)|^2}. \quad (2.39)$$

On the other hand, to see the behavior of the reflection and transmission amplitudes in the gaps of the periodic spectrum, we have to estimate the Chebyshev polynomials outside $[-1, 1]$. By analytical continuation, the relation (2.37) gives $U_n(x) = \sinh((n+1)\operatorname{arcosh} x) / \sinh(\operatorname{arcosh} x)$, so

$$U_n(x) = \sum_{k=0}^n \left(x + \sqrt{x^2 - 1}\right)^{n-2k}.$$

Then we have, for instance, the following estimates

$$n + x^n \leq U_n(x) \leq (n+1) \left(x + \sqrt{x^2 - 1}\right)^n. \quad (2.40)$$

The first inequality yields an upper bound,

$$|t_N(k)|^2 \leq \frac{1}{1 + (N-1 + (\operatorname{Re}(\bar{\varepsilon}R))^{N-1})^2}. \quad (2.41)$$

It is clear that $|t_N(k)|^2 = 1$ holds only if the same is true for $|t(k)|^2$; in all the other cases it behaves as $o\left((\operatorname{Re}(\bar{\varepsilon}R))^{2N-2}\right)$ as $N \rightarrow \infty$. On the other hand, $|t_N(k)|^2 = 0$ holds only if a single scatterer has a full reflection at this energy, otherwise the second inequality of (2.40) together with $|\operatorname{Re}(\bar{\varepsilon}R)| \leq |t(k)|^{-1}$ and the unitarity relation give

$$|t_N(k)|^2 \geq \frac{|t(k)|^{2N}}{|t(k)|^{2N} + N^2|r(k)|^2(1+|r(k)|)^{2N-2}}. \quad (2.42)$$

3 Serial graphs

As we have said we want now to illustrate the above results on several examples which go beyond the usual one-dimensional potential scattering. In this section we shall discuss the situation the serial structure is a graph.

Although nonrelativistic quantum mechanics for quantum particles confined to a graph has been considered already several decades ago in connection with the free-electron models of hydrocarbons [40], it became a subject of intense interest

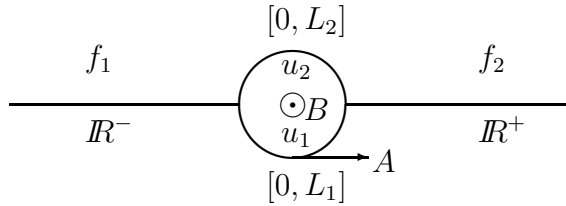


Figure 1: A loop-graph scatterer in a magnetic field

only recently as a tool to describe systems of quantum wires — see [2, 7, 9, 10, 13, 15, 16, 17, 18, 20, 21, 25, 27, 28, 31, 34] and references therein. There are also other systems for which graph description could prove to be useful such as objects composed of carbon nanotubes [14, 30].

Graph systems are attractive because they are often explicitly solvable; on the mathematical level they represent systems of ordinary differential equations in contrast to partial differential equations with nontrivial boundary conditions needed to describe quantum wire systems in higher dimensions. At the same time, the simplified description may still preserve basic features of the real system. Of course, replacing a branched waveguide system by its skeleton graph is a nontrivial approximation, but we shall avoid discussing this point here; some comments can be found in [16, 36] and references given there.

3.1 Loop arrays

In our first example an individual scatterer is a planar loop \mathcal{L} with a pair of external leads placed into a homogeneous magnetic field — *cf.* Fig. 1. We suppose that the field is perpendicular to the graph plane. The corresponding vector potential in the circular gauge is $\vec{A}(\vec{x}) = \left(-\frac{1}{2}By, \frac{1}{2}Bx, 0\right)$ and

$$\int_{\mathcal{L}} \vec{A}(\vec{x}) d\vec{x} = \frac{BS}{L_1 + L_2} = \frac{\Phi}{L_1 + L_2},$$

where S is the loop area, L_j are the lengths of its two branches, and Φ is the corresponding magnetic flux.

Such a scattering system has been considered earlier — see [8, 13, 31] and references therein. The Hilbert space for the graph of Fig. 1 is the orthogonal sum of four L^2 spaces referring to the graph links; its elements will be denoted as (f_1, u_1, u_2, f_2) with the coordinates at the loop taken anticlockwise. We suppose that the particle has a unit charge and apart of the magnetic field it moves as free on the graph. There are various ways how to couple the operators $(-i\partial_x - A)^2$ from different graph links in a self-adjoint way [22, 25, 34]. For the sake of simplicity we restrict ourselves to

the usual δ coupling, *i.e.*, we impose the boundary conditions

$$\begin{aligned} f_1(0) = u_1(0) = u_2(L_2) & \quad -f_1'(0) + u_1'(0) - u_2'(L_2) = \alpha_1 f_1(0), \\ f_2(0) = u_2(0) = u_1(L_1) & \quad f_2'(0) - u_1'(L_1) + u_2'(0) = \alpha_2 f_2(0), \end{aligned} \quad (3.1)$$

where the function and derivative values mean the appropriate one-sided limits. On the other hand, we do not suppose in general that α_1, α_2 and L_1, L_2 are the same.

Substituting into (3.1) the boundary values of the generalized eigenfunctions on the loop, $u_j(x) = A_j e^{-i(A-k)x} + B_j e^{-i(A+k)x}$, $j = 1, 2$, we get a system of six equations. Eliminating from here A_j, B_j we arrive at the relations

$$\begin{aligned} f_2(0) &= \frac{1}{2kD} ((i\alpha_1 B + 2kC) f_1(0) + iB f_1'(0)) \\ f_2'(0) &= \frac{1}{2kD} ((i\alpha_1 \alpha_2 B + 2(\alpha_1 + \alpha_2)kC - 4ik^2 E_- E_+) f_1(0) + (2kC + i\alpha_2 B) f_1'(0)), \end{aligned}$$

determining the transfer matrix, where

$$\begin{aligned} B &= (\varepsilon_{1+} - \varepsilon_{1-})(\varepsilon_{2-} - \varepsilon_{2+}) = 4e^{-i\Phi} \sin kL_1 \sin kL_2, \\ C &= -\varepsilon_{1-} \varepsilon_{2-} + \varepsilon_{1+} \varepsilon_{2+} = 2ie^{-i\Phi} \sin k(L_1 + L_2), \\ D &= \varepsilon_{2+} - \varepsilon_{2-} + \varepsilon_{2+} \varepsilon_{2-} (\varepsilon_{1+} - \varepsilon_{1-}), \\ E_{\pm} &= 1 - \varepsilon_{1\pm} \varepsilon_{2\pm} = 2ie^{-i\Phi/2} e^{\pm ik(L_1 + L_2)/2} \sin \left(\frac{\pm k(L_1 + L_2) - \Phi}{2} \right), \\ \varepsilon_{j\pm} &= e^{i(-A \pm k)L_j}, \quad j = 1, 2. \end{aligned}$$

The reflection and transmission amplitudes are given by

$$\begin{aligned} r(k) &= \frac{-i\alpha_1 \alpha_2 B + k((\alpha_2 - \alpha_1)B - 2(\alpha_1 + \alpha_2)C) + ik^2(4E_- E_+ - B)}{i\alpha_1 \alpha_2 B + k(\alpha_2 + \alpha_1)(2C + B) - ik^2(4E_- E_+ + B + 4C)}, \\ t(k) &= \frac{4ik^2 D e^{-2i\Phi}}{i\alpha_1 \alpha_2 B + k(\alpha_2 + \alpha_1)(2C + B) - ik^2(4E_- E_+ + B + 4C)}, \end{aligned} \quad (3.2)$$

respectively. Since B, C, E_{\pm} as well as D^2 are 2π -periodic functions of the magnetic flux, the same is valid for the reflection and transmission *probabilities*. Recall that if we put $e = \hbar = c = 1$, then 2π is the magnetic flux quantum in these units.

3.2 Band spectrum of an infinite loop array

We illustrate the relation of transmission probabilities of a finite array of loops and the spectrum of the corresponding infinite system on Fig. 2. As already mentioned $|t_N(k)|^2$ is a 2π -periodic function and because the condition (2.35) determining the band spectrum of the infinite system can be reformulated as $0 < |\text{Re}(\bar{\varepsilon}R)| < 1$ we show dependence on Φ only in the range $[0, 2\pi]$ ($|\text{Re}(\bar{\varepsilon}R)|$ is also a 2π -periodic

function). We choose loops with different L_1, L_2 and α_1, α_2 . Even for a relatively small number of loops $N = 6$ the values of $|t_N(k)|^2$ are clearly nonzero in areas of parameters Φ and k where there are bands of the infinite system and negligible where there are gaps.

3.3 Comb graphs

Our next example concerns the case of a comb-shaped graph, *i.e.*, a line with a finite number N of identical appendices attached to it at equally spaced points. Such systems have been discussed recently [42] following earlier studies of a single-stub waveguide [37, 43, 44, 47].

Comparing to the previous work and the preceding example, we shall discuss comb-shaped graphs in a more thorough way. First of all, instead of the δ -coupling used above (or the Griffith's boundary conditions in the terminology of [42]) we allow for the most general self-adjoint way in which the stubs can be attached to continuous wavefunctions on the line. This amounts to imposing at the junctions the boundary conditions adopted from an earlier treatment of the T-shaped graph [25]. Should the Hamiltonian be time-reversal invariant, the junction is then characterized by three real parameters. In this framework we are able to handle imperfect contacts [17]; moreover, it is straightforward to modify the results derived below to graphs with a δ' -coupling which corresponds to the situation where the junction itself represents a complicated geometric scatterer (see [9, 16], more about that will be said in the next section). Computing the S-matrix we also assume that the particle is under influence of a potential on the stubs; this makes it possible to investigate how the band-form zones of high transmission which arise for $N \gg 1$ change when an external field is applied.

The formula derived in the previous section allows us to express the transmission and reflection probabilities. In addition to them, one is able to generalize the result of [25] to the present situation and to find an explicit Krein-formula expression for the resolvent of the comb-graph Hamiltonian. This allows us to study their resonance structure of the problem which arises from perturbation of the disconnected-stub discrete spectrum embedded into the continuum of the line motion. The mentioned expression yields an equation from which the resolvent singularities on the second sheet can be found.

After this introduction, let us describe the model. For a greater generality we suppose first that the appendices are not necessarily identical. The graph Γ_N will therefore consist of a line with a finite sequence $\{(s-1)\ell\}_{s=1}^N$ of points at which appendices of finite lengths L_s are attached (see Fig.3). The state Hilbert space of the problem is then $\mathcal{H} \equiv L^2(\Gamma_N) := L^2(\mathbb{R}) \oplus \left(\bigoplus_{s=1}^N L^2(0, L_s)\right)$; we shall write its elements as columns

$$\psi = \begin{pmatrix} f \\ u_1 \\ \vdots \\ u_N \end{pmatrix}.$$

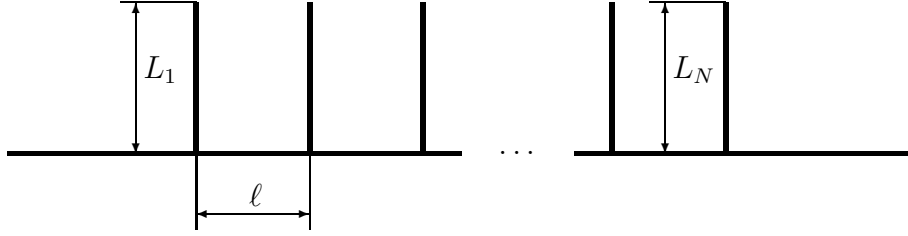


Figure 3: A comb-shaped graph

We suppose that the motion at the backbone line is free while the particle is exposed to potentials V_s on the “teeth”; hence the Hamiltonian of a nonrelativistic particle of mass $m = 1/2$ living on Γ_N acts as

$$(H\psi)_1(x) := -f''(x), \quad (H\psi)_{s+1}(x) := (-u_s'' + V_s u_s)(x), \quad s = 1, \dots, N, \quad (3.3)$$

out of the junctions. To make it a self-adjoint operator one has to choose again properly the boundary conditions which couple the wavefunctions at the branching points of the graph in such a way that the probability current conservation at the vertices is conserved. As we have said, we shall require continuity of the line component f of ψ at the junctions; to keep a manageable number of parameters we assume the Dirichlet conditions at the end of the stubs. Consequently, the domain of the Hamiltonian consists of all $\psi \in \mathcal{H}$ with $f \in AC^2(\mathbb{R})$ and $u_s \in AC^2(0, L_s)$ satisfying the conditions [25]

$$\begin{aligned} f((s-1)\ell+) &= f((s-1)\ell-) =: f((s-1)\ell), \\ u_s(0) &= b_s f((s-1)\ell) + c_s u_s'(0), \\ f'((s-1)\ell+) - f'((s-1)\ell-) &= d_s f((s-1)\ell) - b_s u_s'(0), \\ u_s(L_s) &= 0 \end{aligned} \quad (3.4)$$

for $s = 1, \dots, N$. In general, b_s may be complex, however, we restrict from the start to Hamiltonians which are time-reversal invariant and suppose that the coefficient matrices $\mathbb{K}_s = \begin{pmatrix} b_s & c_s \\ d_s & -b_s \end{pmatrix}$ are real. The s -th appendix is decoupled from the line by putting $b_s = 0$; it is then described by the operator $h_{c_s} := -\frac{d^2}{dx^2} + V_s$ specified by the decoupled condition

$$u_s(0) - c_s u_s'(0) = 0 \quad (3.5)$$

at the junction.

In what follows we concentrate on the finite periodic case where $L_s = L$, $V_s = V$, and $\mathbb{K}_s = \mathbb{K}$; the operator specified by the boundary conditions (3.4) will be denoted as $H_N \equiv H_N(\mathbb{K}, V)$. The potential V is supposed to belong to $L^1(0, L)$.

3.4 Scattering on a comb graph

To write the scattering matrix we need some notation. Let u_L be the unique solution to the appendix Schrödinger equation,

$$-u_L'' + Vu_L = k^2 u_L \quad (3.6)$$

with the energy k^2 and the normalized Dirichlet condition at the outer endpoint, $u_L(L) = 1 - u_L'(L) = 0$. If all the junctions are described by the parameters b, c, d in (3.4), we put

$$\beta := \frac{d}{2k} + \frac{b^2}{2k} \left(\frac{u_L'}{cu_L' - u_L} \right) (0), \quad \zeta := \cos k\ell + \beta \sin k\ell, \quad (3.7)$$

and denote again $\varepsilon := e^{ik\ell}$. For a single stub, $s = N = 1$, we insert a generalized eigenvector of the form $\begin{pmatrix} f \\ \alpha u_1 \end{pmatrix}$ into the boundary conditions (3.4) and express $f(0+)$, $f'(0+)$ by means of the left-sided limits; this yields the single-element transfer matrix which can be with the help of (3.7) written as

$$L_\beta = \begin{pmatrix} 1 & 0 \\ 2k\beta & 1 \end{pmatrix},$$

so $R = 1 + i\beta$ and $S = i\beta$. Furthermore, $Re(\bar{\varepsilon}R) = \zeta$. Using then the explicit expression (2.30) of the phase factor together with (2.31) and (2.32), we may write the left-to-right scattering amplitudes as

$$r_N = \frac{i\beta U_{N-1}(\zeta)}{\varepsilon U_{N-2}(\zeta) - (1+i\beta)U_{N-1}(\zeta)}, \quad t_N = -\frac{\varepsilon^{1-N}}{\varepsilon U_{N-2}(\zeta) - (1+i\beta)U_{N-1}(\zeta)}. \quad (3.8)$$

In particular, the reflection and transmission probabilities are

$$|t_N(k)|^2 = 1 - |r_N(k)|^2 = \frac{1}{1 + \beta^2 U_{N-1}(\zeta)^2}. \quad (3.9)$$

In order to illustrate the usefulness of the formulas (2.31)–(2.33), we present in Appendix A two other ways to derive the relations (3.8).

Let us now illustrate how the the transmission probability depends on the number of the teeth and the parameters of the junctions. Fig. 4 shows a typical example of the situation. For a certain set of parameters b, c , and d we compare $|t(k)|^2$ for one and seven appendices with an infinite array of them. The band spectrum is marked by thick lines above. The suppression of transmission coefficient at those values of k where the infinite system shows gaps is evident even for a relatively small number of elementary scatterers, $N = 7$. In each band we distinguish $N - 1$, *i.e.* six values of k_i when $|t(k_i)|^2 = 1$ as it should be – *cf.* (2.37). In addition the first and third band contain an additional value of k_a for which $|t(k_a)|^2 = 1$ and these values coincide with the values of k for which a single appendix allows a perfect transmission. The values of k for which the reflection is total fall into gaps of the infinite system as it should be (*cf.* the end of sec. 2.4).

3.5 The resolvent poles

The energy dependence of the transmission probability through the comb graph is related to its resonance structure which in turn comes from perturbation of embedded eigenvalues of $H_N(0, V)$ referring to the stubs by the coupling between the line and the “teeth”. The resonances are conventionally associated with the poles of the analytically continued resolvent; we are going to show now how they can be found.

As in the particular case $N = 1$ discussed in [25], one can derive an expression for the resolvent $(H_N - z)^{-1}$ of the operator $H_N(\mathbb{K}, V)$ by means of Krein’s formula [5, Appendix A]: it is an integral operator with the kernel

$$(H_N - z)^{-1}(x, y) = (H_0 - z)^{-1}(x, y) + \sum_{m,n=1}^{2N} \lambda_{mn} F_m(x, z) F_n(y, z); \quad (3.10)$$

in this relation H_0 is a suitable comparison operator and the vectors F_m satisfying $\overline{F_m(x, \bar{z})} = F_m(z)$ belong to the deficiency subspace (for a given complex energy z) of the maximum common restriction of H_N and H_0 .

As usual we put $k := \sqrt{z}$. We choose for H_0 the fully decoupled operator with $b_s = c_s = d_s = 0$, $s = 1, \dots, N$. Its resolvent can be written down explicitly; its kernel is a $(N+1) \times (N+1)$ matrix

$$(H_0 - z)^{-1}(x, y) = \begin{pmatrix} R_1(x, y; z) & 0 & \dots & 0 \\ 0 & -\frac{u_{0,1}(x_<)u_{L,1}(x_>)}{W(u_{0,1}, u_{L,1})} & \dots & 0 \\ \vdots & & \ddots & \vdots \\ 0 & & & -\frac{u_{0,N}(x_<)u_{L,N}(x_>)}{W(u_{0,N}, u_{L,N})} \end{pmatrix}, \quad (3.11)$$

where $W(u_{0,n}, u_{L,n})$ is the Wronskian of the solutions $u_{0,n}$ and $u_{L,n}$ to $-u'' + V_n u = k^2 u$ specified by the boundary conditions $u_{0,n}(0) = 0$ and $u_{L,n}(L_n) = 0$, respectively. The symbols $x_<$ and $x_>$ mean respectively the smaller and larger of the variables x, y , and

$$R_1(x, y; z) := \frac{i}{2k} e^{ik|x-y|} \quad (3.12)$$

is the free resolvent kernel on the line. A natural choice of the deficiency vectors is the following:

$$F_n(x) := \begin{pmatrix} R_1(x, (n-1)\ell; z) \\ 0 \\ \vdots \\ 0 \end{pmatrix}, \quad F_{n+N}(x) := \begin{pmatrix} 0 \\ \vdots \\ u_{L,n}(x, z) \\ \vdots \\ 0 \end{pmatrix} \quad (3.13)$$

for $n = 1, \dots, N$. To find the coefficients λ_{mn} we use the fact that for z of the resolvent set the resolvent maps $L^2(\Gamma_N)$ onto the domain of H_N . Hence the

components of the vector at the $lhsof$

$$\begin{pmatrix} f \\ u_1 \\ \vdots \\ u_N \end{pmatrix} = (H_N - z)^{-1} \begin{pmatrix} g \\ v_1 \\ \vdots \\ v_N \end{pmatrix} \quad (3.14)$$

have to satisfy the boundary conditions (3.4) for arbitrary (square integrable) functions g, v_1, \dots, v_N . For the sake of brevity we introduce

$$h_n := \int_{\mathbb{R}} R_1(y, (n-1)L; z) g(y) dy, \quad h_{n+N} := \int_0^{\ell_n} u_n(y, z) v_n(y) dy$$

with $n = 1, \dots, N$; they represent $2N$ independent quantities. By direct computation we find then the needed boundary values from (3.10)–(3.14),

$$\begin{aligned} f((s-1)\ell) &= h_s + \frac{i}{2k} \sum_{l=1}^{2N} \left(\sum_{n=1}^N \varepsilon^{|s-n|} \lambda_{nl} \right) h_l, \\ f'((s-1)\ell+) &= \int_{\mathbb{R}} \frac{\partial R_1(x, y; z)}{\partial x} \Big|_{x=(s-1)\ell+} g(y) dy + \\ &\quad + \frac{1}{2} \sum_{l=1}^{2N} h_l \left(- \sum_{n=1}^{s-2} \lambda_{nl} \varepsilon^{s-n} + \sum_{n=s-1}^N \lambda_{nl} \varepsilon^{n-s} \right), \\ f'((s-1)\ell-) &= \int_{\mathbb{R}} \frac{\partial R_1(x, y; z)}{\partial x} \Big|_{x=(s-1)\ell-} g(y) dy + \\ &\quad + \frac{1}{2} \sum_{l=1}^{2N} h_l \left(- \sum_{n=1}^{s-1} \lambda_{nl} \varepsilon^{s-n} + \sum_{n=s}^N \lambda_{nl} \varepsilon^{n-s} \right), \\ u_s(0) &= u_{L,s}(0) \sum_{k=1}^{2N} h_k \lambda_{N+s,k}, \\ u'_s(0) &= \frac{1}{u_{L,s}(0)} h_{N+s} + u'_{L,s}(0) \sum_{k=1}^{2N} h_k \lambda_{N+s,k}, \end{aligned} \quad (3.15)$$

where $s = 1, \dots, N$ and $\varepsilon := e^{ik\ell}$. Substituting from here to (3.4) and using the fact that h_n are independent we arrive at the following system of equations

$$\sum_{n=1}^N \frac{ib_s}{2k} \varepsilon^{|s-n|} \lambda_{nl} + (c_s u'_{L,s}(0) - u_{L,s}(0)) \lambda_{N+s,l} = \begin{cases} -b_s & l = s \\ -\frac{c_s}{u_{L,s}(0)} & l = N+s \\ 0 & \text{otherwise} \end{cases} \quad (3.16)$$

$$\sum_{n=1}^N \left(\frac{id_s}{2k} \varepsilon^{|s-n|} + \delta_{sn} \right) \lambda_{nl} - b_s u'_{L,s}(0) \lambda_{N+s,l} = \begin{cases} -d_s & l = s \\ \frac{b_s}{u_{L,s}(0)} & l = N+s \\ 0 & \text{otherwise} \end{cases}$$

with $s = 1, \dots, N$, $l = 1, \dots, 2N$. If we arrange the sought coefficients in the following way,

$$\lambda_{1,1}, \dots, \lambda_{2N,1}, \lambda_{1,2}, \dots, \lambda_{2N,2}, \dots, \lambda_{1,2N}, \dots, \lambda_{2N,2N},$$

the matrix of the system (3.16) is block diagonal with $2N$ same $2N \times 2N$ blocks. This is important because we are looking for singularities of the resolvent (3.10) which occur at the points where the coefficients λ_{mn} are singular. The latter are solutions to the linear system (3.16), and therefore they have the same denominator; looking for its zeros it is sufficient to inspect the determinant of a single block,

$$\begin{vmatrix} \frac{ib_s}{2k} \varepsilon^{|s-n|} & \vdots & (c_s u'_{L,s} - u_{L,s})(0) \delta_{s,N-n} \\ \dots & \dots & \dots \\ \frac{id_s}{2k} \varepsilon^{|s-n|} + \delta_{s-N,n} & \vdots & -b_{s-N} u'_{L,s-N}(0) \delta_{s,n} \end{vmatrix}.$$

For a non-real z we have

$$(c_s u'_{L,s} - u_{L,s})(0) \neq 0 \quad \text{and} \quad b_s u'_{L,s}(0) \neq 0$$

for all $s = 1, \dots, N$, since otherwise the decoupled stub Hamiltonian with the appropriate boundary condition at $x = 0$ would have a complex eigenvalue which is clearly impossible. Vanishing of the above determinant is then equivalent to

$$D_N := \det (i\beta_n \varepsilon^{|s-n|} + \delta_{s,n}) = 0,$$

where

$$\beta_n := \frac{d_n}{2k} + \frac{b_n^2}{2k} \left(\frac{u'_{L,n}}{c u'_{L,n} - u_{L,n}} \right) (0).$$

Up to now the stubs could be mutually different. We shall evaluate the determinant in the finitely periodic case, $\beta_n = \beta$ for $n = 1, \dots, N$. Then D_N can be written as

$$D_N = \frac{1}{1-\varepsilon^2} \left[(i\beta(1-\varepsilon^2) + 1) \tilde{D}_{N-1} - \varepsilon^2 \tilde{D}_{N-2} \right], \quad (3.17)$$

where

$$D_0 = i\beta + 1, \quad D_1 = 1 + 2i\beta - \beta^2(1-\varepsilon^2), \quad (3.18)$$

and the quantities satisfy the recursive relation

$$\bar{\varepsilon} \tilde{D}_N - 2z \tilde{D}_{N-1} + \varepsilon \tilde{D}_{N-2} = 0. \quad (3.19)$$

Comparing this to the relations between Chebyshev polynomials we find

$$D_N = -\varepsilon^{N-1} (\varepsilon U_{N-2}(\zeta) - (1+i\beta) U_{N-1}(\zeta)), \quad (3.20)$$

since (3.17) is a linear difference equation of the second order with constant coefficients which has for the given initial conditions (3.18) a unique solution.

We see that $D_N(k) = 0$ if and only if the same is true for the denominator of the reflection and transmission amplitude. Hence the poles of the continued resolvent and of the S-matrix generically coincide. It might be that some of them vanish due to a zero in the numerator, however, this can happen in isolated points only because the numerators are analytical functions of the coupling parameters, and there is a one-to-one correspondence between the pole trajectories with respect to the coupling constant and the embedded eigenvalues of the decoupled Hamiltonian $H(0, V)$.

3.6 Band spectrum of an infinite comb and resonances

We discuss only the case of free appendices here, *i.e.* $V_s = 0$. Investigation of non-zero potentials represents no complication in general conception. Typical spectra of an infinite comb are presented on Fig. 5. The parameters of such a structure could be divided into two groups, *viz.* ℓ, L and b, c, d . The dependence on ℓ is rather simple; a change of ℓ results in scaling of spectrum in k . This is the consequence of the fact that the transfer matrix T depends only on the product $k\ell$. This is the reason why we show all the spectra for $\ell = 1$ only. The dependence on L is more complicated as can be inferred from Fig. 5.

A striking feature of such a spectrum are sudden transitions of bands to gaps or vice versa at $k\ell = n\pi$, $n \in \mathbb{Z}$ for almost all L . This can be understood, if we write down the Bloch condition explicitly as

$$\beta(k) \sin(k\ell) + \cos(k\ell) = \cos(\theta).$$

Clearly, this is always fulfilled for $k\ell = n\pi$, unless β has a singularity at $n\pi/\ell$. Therefore $k = n\pi/\ell$ belongs always to the band in this case. The situations when $\beta(n\pi/\ell)$ is infinite requires a further analysis. An effect of a small change ϵ in k can be estimated from $\beta(k + \epsilon)\epsilon\ell + 1 = (-1)^n \cos(\theta)$. With exception of points where $\beta(n\pi/\ell) = 0$, small change of ϵ does not change the sign of β , while the change of sign of ϵ leads to the change of sign of $\beta(k + \epsilon)\epsilon\ell$. Only at vicinity of points where $\beta(n\pi/\ell) = 0$ can the sign of $\beta(k + \epsilon)\epsilon\ell$ rest unchanged, *cf.* Fig 5.

Of the three parameters determining the coupling of an appendix to the backbone line *i.e.* b, c, d , we find b as the most suitable to begin with. Putting $b = 0$ switches effectively off the appendices as already mentioned in sec. 3.2. This implies that we have eigenvalues k_n^2 embedded in the continuum, where k_n are solutions of (3.5). These values of momentum play an important role from three points of view. First, k_n 's are the values for which $u_L(0) = 0$ and the number of zeros of u increases by one when k passes to higher values; this means that the whole \mathbb{R}^+ is divided into disjoint intervals by these values (for a given L). On the other hand, a band can belong to two intervals (although this happens only for some L) and states of the same band can be described by wave functions with different number of zeros of u 's. Also, and this situation is far more frequent, one interval can contain two or more band, so that the number of zeros of u is not directly related to the ordinal number of a band.

In order to reveal the second role of these values k_n 's, we have to return to finite number of appendices attached to the line. If we begin with one appendix only, direct calculation shows that $t(k_n) = 0$ and $r(k_n) = -1$. Therefore, regardless of the number of appendices N the full reflection takes place, *i.e.* $t_N = 0, r_N = -1$.

We close this section with discussion of scattering resonances of our system. Recently, it was shown [11] that there is certain “band” structure in the spectrum of resonances and that this spectrum converges to the energy band spectrum of the infinite periodic system in the limit of an infinite number of scatterers. The authors also show that one should expect $N - 1$ resonances in each band if the system consists of N identical cells. These conclusions are in accordance with our results but for one difference – the number of resonances in a band is $2N - 1$. It is a consequence of the fact that the origin of resonances is twofold here. $N - 1$ resonances comes from the spacial order of our periodical structure as in [11] and the remaining N ones have their origin in k_n^2 , which is an N -fold eigenvalue for the case of $b = 0$. As $|b|$ grows this degeneracy is lifted and we find N resonances in the vicinity of k_n^2 . This is the third role of k_n . The $N - 1$ resonances related to the spatial setting travel from $-\infty$ and for small b these two sets are well separated as is shown on Fig. 6.

There are situations when a resonance or a bound state appears at $k = 0$. The manifestation of this instance is that $|t(0)|^2 = 1$. This can take place even in the case of one appendix. The expression (5) of [25] with explicit form of $u_L(0)$ shows that this can happen as soon as the condition

$$d(c + L) + b^2 = 0$$

is fulfilled. Provided that this condition holds, there is perfect transmission at $k = 0$ for any number of appendices, *i.e.* $t_N(0) = 1$. Besides this there could be other situations when $t_N(0) = 1$ for $N > 1$. If there exists such an $n = 1, \dots, N - 1$ that

$$\cos\left(\frac{n\pi}{N}\right) = 1 + \frac{(dc + dL + b^2)\ell}{2(c + L)},$$

we have again $t_N(0) = 1$. This corresponds to $U_{N-1}(\zeta(0)) = 0$ in (3.9). Direct inspection confirms that the wave function does not belong to $L^2(\Gamma_N)$ and that these states are resonances (and not bound states).

4 Serial structures of mixed dimensionality

In this section we want to treat the situation when the scatterers connected by single-mode leads have a higher dimension. For the sake of simplicity, we shall consider only the simplest possibility when the dimension is two, *i.e.*, the scatterer is a surface. Such systems can be realized in both the solid state (recall, *e.g.*, the “bamboo defects” in nanotubes [32]) and electromagnetism (for flat resonators), but we avoid discussing examples and the conditions under which these models are realistic. We suppose that the surface is smooth, bounded, and connected, with or without the boundary. Although it makes no difficulty to let the particle on the

surface interact with an external potential field, we will regard it as free, *i.e.*, its Hamiltonian will be (in appropriate units) just the corresponding Laplace–Beltrami operator.

4.1 Coupling of leads to a surface

The basic question for the described serial structures is the way in which the leads are coupled to the scatterers. The physical condition is again a conservation of the probability current, which translates into the self-adjointness requirement of the corresponding Hamiltonian. Since the coupling is local, we may disregard geometrical peculiarities of the lead and the surface and consider the setting when a halfline is attached to a plane. The state Hilbert space is then $L^2(\mathbb{R}^-) \oplus L^2(\mathbb{R}^2)$ and the Hamiltonian acts on its elements $\begin{pmatrix} \phi_1 \\ \phi_2 \end{pmatrix}$ as $\begin{pmatrix} -\phi_1'' \\ -\Delta\phi_2 \end{pmatrix}$. To make it self-adjoint one has to impose suitable boundary conditions which couple the wavefunctions at the junction. A general solution to this problem is given in Ref.[21]. The conditions are of the form

$$\phi_1'(0-) = A\phi_1(0-) + BL_0(\phi_2), \quad L_1(\phi_2) = C\phi_2(0-) + DL_0(\phi_2) \quad (4.1)$$

together with several “exceptional” classes, where

$$L_0(\phi_2) = \lim_{r \rightarrow 0^+} \frac{\phi_2(\vec{x})}{\ln r},$$

$$L_1(\phi_2) = \lim_{r \rightarrow 0^+} (\phi_2(\vec{x}) - L_0(\phi_2) \ln r)$$

with $r := |\vec{x}|$ are the generalized boundary values in the plane, and the coefficients A, B, C, D depend on four real parameters; evaluating the boundary form, it is straightforward to see that they satisfy restrictions

$$A, D \in \mathbb{R} \quad B = 2\pi\overline{C}. \quad (4.2)$$

A disadvantage of this result is that it tells us nothing about physical relevance of the coefficients values in the boundary conditions (4.1). The choice of the coupling depends on particular properties of the junction it models, of course, but one would like to select a subclass representing a “natural” coupling. One way to achieve this goal was suggested in [23]: comparing the scattering matrix of the junction given by (4.1) with the low-energy behavior of scattering in the system of a plane to which a cylindrical “tube” is attached, and taking into account the condition (4.2), we arrive at the identification

$$A = \frac{1}{2\rho}, \quad B = \sqrt{\frac{2\pi}{\rho}}, \quad C = \frac{1}{\sqrt{2\pi\rho}}, \quad D = -\ln \rho, \quad (4.3)$$

where ρ is the contact radius. Physical relevance of these conditions was illustrated in [23] by explaining the experimentally observed distribution of resonances in a microwave resonator with a thin antenna. Motivated by this, we will use in the following (4.1) and (4.3) to describe the coupling between the leads and the scatterers.

4.2 The single–element S–matrix

Using the local character of the boundary conditions derived above we apply them to coupling of a pair of halfline leads to an arbitrary surface G . The only restriction is that the junction may not belong to the boundary of G if it has any. We shall compute the transfer and scattering matrices for such a system.

As we have said the Hamiltonian is a Laplace–Beltrami operator on the state Hilbert space $L^2(G)$ of the scatterer. We shall characterize it by its Green’s function $G(\cdot, \cdot; k)$, *i.e.*, the integral kernel of its resolvent which exists whenever k^2 does not belong to the spectrum. Its actual form depends on the geometry of G but we shall not need it. What is important is the character of its singularity. As a smooth manifold, G admits in the vicinity of any point a local Cartesian chart and the Green’s function behaves as that of Laplacian in the plane,

$$G(x, y; k) = -\frac{1}{2\pi} \ln|x-y| + \mathcal{O}(1), \quad |x-y| \rightarrow 0. \quad (4.4)$$

Looking for scattering solutions to the Schrödinger equation, we need a general solution to the Laplace–Beltrami equation on G for the energy k^2 . Without loss of generality, we may write it as

$$u(x) = a_1 G(x, x_1; k) + a_2 G(x, x_2; k), \quad (4.5)$$

where x_1, x_2 are two different points of G at which the leads are attached. The generalized boundary values (labelled by the point at which they are taken) of this solution are then

$$L_0[x_j] = -\frac{a_j}{2\pi}, \quad L_1[x_j] = a_j \xi(x_j, k) + a_{3-j} G(x_1, x_2; k) \quad (4.6)$$

for $j = 1, 2$, where

$$\xi(x_j; k) = \lim_{x \rightarrow x_j} \left[G(x, x_j; k) + \frac{\ln|x-x_j|}{2\pi} \right]. \quad (4.7)$$

Next we denote the wavefunction on the j -th lead as u_j . For simplicity we use the abbreviations u_j, u'_j for its boundary values; then the boundary conditions (4.1) yield

$$\begin{aligned} u'_1 &= A_1 u_1 - \frac{B_1 a_1}{2\pi}, & a_1 \xi_1 + a_2 g &= C_1 u_1 - \frac{D_1 a_1}{2\pi}, \\ u'_2 &= -A_2 u_2 + \frac{B_2 a_2}{2\pi}, & a_2 \xi_2 + a_1 g &= C_2 u_2 - \frac{D_2 a_2}{2\pi}, \end{aligned}$$

where $g := G(x_1, x_2; k)$. In the the first equation of the second pair we have changed sign, because the second lead is identified with \mathbb{R}^+ . It is straightforward to rewrite

these equations as a linear system with the unknown u_2, u_2', a_1, a_2 and to solve it; this gives in particular the transfer matrix,

$$L = \frac{1}{gC_2} \begin{pmatrix} C_1 Z_2 + 2\pi \frac{A_1}{B_1} \Delta & -2\pi \frac{\Delta}{B_1} \\ B_2 C_2 \left(\frac{C_1}{2\pi} - Z_1 \frac{A_1}{B_1} \right) - C_1 A_2 Z_2 - 2\pi \frac{A_1 A_2}{B_1} \Delta & 2\pi \frac{A_2}{B_1} \Delta + \frac{B_2 C_2 Z_1}{B_1} \end{pmatrix}, \quad (4.8)$$

where $Z_j := \frac{D_j}{2\pi} + \xi_j$ and $\Delta := g^2 - Z_1 Z_2$. Using (4.2) we find easily

$$\det L = -\frac{B_2 C_1}{B_1 C_2} = -\frac{\overline{C_2} C_1}{C_1 C_2}, \quad (4.9)$$

so $\det L = 1$ if the junctions are identical or the coefficients C_j are real. The second possibility is if the couplings are invariant with respect to the time reflection, which we shall suppose in the following. In that case the transfer matrix simplifies to the form

$$L = \frac{1}{g} \begin{pmatrix} Z_2 + \frac{A}{C^2} \Delta & -2\frac{\Delta}{C^2} \\ C^2 - A(Z_1 + Z_2) - \frac{A^2}{C^2} \Delta & \frac{A}{C^2} \Delta + Z_1 \end{pmatrix}, \quad (4.10)$$

in particular

$$L = \frac{1}{g} \begin{pmatrix} Z_1 + \pi \Delta & -2\pi \rho \Delta \\ \frac{1}{2\rho} \left(\frac{1}{\pi} - Z_1 - Z_2 - \pi \Delta \right) & Z_1 + \pi \Delta \end{pmatrix} \quad (4.11)$$

for the physically most interesting class of couplings (4.3). The S-matrix of our geometric scatterer is then given by the relations (2.31) and (2.32); in the case (4.11) we have

$$r(k) = -\frac{\pi \Delta + Z_1 + Z_2 - \pi^{-1} + 2ik\rho(Z_2 - Z_1) + 4\pi k^2 \rho^2 \Delta}{\pi \Delta + Z_1 + Z_2 - \pi^{-1} + 2ik\rho(Z_1 + Z_2 + 2\pi \Delta) - 4\pi k^2 \rho^2 \Delta}, \quad (4.12)$$

$$t(k) = -\frac{4ik\rho g}{\pi \Delta + Z_1 + Z_2 - \pi^{-1} + 2ik\rho(Z_1 + Z_2 + 2\pi \Delta) - 4\pi k^2 \rho^2 \Delta}.$$

To make use of these formulas, we need to know g, Z_1, Z_2, Δ as functions of the momentum k . By assumption the manifold G is compact, so the spectrum $\{\lambda_n\}_{n=1}^{\infty}$ of the Hamiltonian is purely discrete and the corresponding eigenfunctions $\{\phi(x)_n\}_{n=1}^{\infty}$ form an orthonormal basis in $L^2(G)$. The usual Green's function expression then gives

$$g(k) = \sum_{n=1}^{\infty} \frac{\phi_n(x_1) \overline{\phi_n(x_2)}}{\lambda_n - k^2}. \quad (4.13)$$

To express the remaining three values we have to compute the regularized limit (4.7). Expanding the logarithm into the Taylor series, we can rewrite the sublimit expression as

$$G(x_j + \sqrt{\varepsilon}n, x_j; k) + \frac{\ln \sqrt{\varepsilon}}{2\pi} = \sum_{n=1}^{\infty} \left(\frac{\phi_n(x_j + \sqrt{\varepsilon}n) \phi_n(x_j)}{\lambda_n - k^2} - \frac{(1-\varepsilon)^n}{4\pi n} \right),$$

where n is a unit vector in the local chart around the point x_j . Unfortunately, interchanging the limit with the sum is not without risk since the latter does not converge uniformly. To see that the result may indeed depend on the regularization procedure, it is sufficient to replace $\sqrt{\varepsilon}$ by $c\sqrt{\varepsilon}$ at the *lhs*. To make idea about this non-uniqueness, let us compute the difference

$$\xi(x_j, k) - \xi(x_j, k') = \lim_{\varepsilon \rightarrow 0^+} \sum_{n=1}^{\infty} \left(\frac{\phi_n(x_j + \sqrt{\varepsilon n}) \overline{\phi_n(x_j)}}{\lambda_n - k^2} - \frac{\phi_n(x_j + \sqrt{\varepsilon n}) \overline{\phi_n(x_j)}}{\lambda_n - k'^2} \right).$$

This sum is already uniformly convergent, because by standard semiclassical estimates [38, XIII.16] the sequence $\{\|\phi_n\|_{\infty}\}_{n=1}^{\infty}$ is bounded with our assumptions and $\lambda_n = 4\pi|G|^{-1}n + \mathcal{O}(1)$ as $n \rightarrow \infty$, so

$$\frac{1}{\lambda_n - k^2} - \frac{1}{\lambda_n - k'^2} \sim \frac{1}{n^2},$$

and therefore

$$\xi(x_j, k) - \xi(x_j, k') = \sum_{n=1}^{\infty} \left(\frac{|\phi_n(x_j)|^2}{\lambda_n - k^2} - \frac{|\phi_n(x_j)|^2}{\lambda_n - k'^2} \right). \quad (4.14)$$

From the same reason

$$\tilde{\xi}(x_j, k) := \sum_{n=1}^{\infty} \left(\frac{|\phi_n(x_j)|^2}{\lambda_n - k^2} - \frac{1}{4\pi n} \right) \quad (4.15)$$

makes sense and $\xi(x_j, k) - \tilde{\xi}(x_j, k)$ is independent of k . We have therefore

$$\xi(x_j, k) = \sum_{n=1}^{\infty} \left(\frac{|\phi_n(x_j)|^2}{\lambda_n - k^2} - \frac{1}{4\pi n} \right) + c(G). \quad (4.16)$$

The constant depends only on the manifold G we will neglect it in the following, because its nonzero value means just a coupling constant renormalization: D_j has to be changed to $D_j + 2\pi c(G)$. For a flat rectangular G we found in [23] an agreement with the experiment using $c(G) = 0$.

4.3 A “bubble” on the line

To make the above consideration more concrete, we shall concentrate in the rest of this section on a single example. We are going to consider the case when G is a sphere of radius R with the leads attached at the poles, which is the system proposed by Kiselev [33]. The most important result of this paper was that apart of the resonances coming from the bound states on the sphere, such a scatterer has the high-energy behavior similar to that of the so-called δ' interaction [6, 9, 19], *i.e.*, the transmission probability *decays* as E^{-1} for $E \rightarrow \infty$. This was established in Ref. [33] up to a logarithmic correction. The difference here is that we shall use the physically interesting coupling (4.3), while [33] employed a two-dimensional subset

of the conditions (4.1) disjoint with the above one. This leads to a different S–matrix, and while the indicated high–energy behavior remains preserved, the argument used in [33] to demonstrate it has to be changed in numerous places; this is why we present its modified version here.

The sphere Hamiltonian is chosen in the standard way. Using the spherical coordinates, we write it as

$$H_G = \frac{1}{R^2} \frac{\partial^2}{\partial \theta^2} + \frac{\cot \theta}{R^2} \frac{\partial}{\partial \theta} + \frac{1}{R^2 \sin^2 \theta} \frac{\partial^2}{\partial \varphi^2} \quad (4.17)$$

with the usual domain. For the sake of simplicity we put $R = 1$ in the following; the results for a general R can be obtained by a scaling transformation. The spectrum of H_G then consists of the eigenvalues are $\lambda_{l,m} = l(l+1)$, $l = 0, 1, \dots$, $m = -l, -l+1, \dots, l$ of multiplicity $2l+1$ to which the eigenfunctions

$$\phi_l^m(\theta, \psi) = \sqrt{\frac{(2l+1)(l-|m|)!}{4\pi(l+|m|)!}} P_l^{|m|}(\cos \theta) e^{im\varphi}$$

correspond. The junctions x_1, x_2 we place at the points $\theta = 0$ and $\theta = \pi$, respectively, where

$$P_l^{|m|}(\pm 1) = (-1)^l \delta_{0,|m|},$$

so only states with $m = 0$ can be coupled to the leads. To express the S–matrix, we need the quantities

$$g(k) = \frac{1}{4\pi} \sum_{l=1}^{\infty} \frac{2l+1}{l(l+1) - k^2} (-1)^l, \quad (4.18)$$

$$Z_j(k) = Z(k) := \frac{1}{4\pi} \sum_{l=1}^{\infty} \left(\frac{2l+1}{l(l+1) - k^2} - \sum_{j=0}^{2l} \frac{1}{l^2 + j + 1} \right) - \frac{\ln \rho}{2\pi} + c(G), \quad (4.19)$$

where ρ is the junction diameter which is supposed to be the same for $j = 1, 2$. The relations (4.12) yield, in particular, the transmission probability in the form

$$t(k) = \frac{4\pi i k \rho g(k)}{1 - 2\pi Z(k)(1 + 2ik\rho) - \pi^2 \Delta(k)(1 + 2ik\rho)^2}, \quad (4.20)$$

where $\Delta(k) = (g(k) - Z(k))(g(k) + Z(k))$.

To prove that (4.20) behaves as indicated above at large values of $E = k^2$, we need several auxiliary results.

Lemma 4.1 *The function $Z(\cdot) + (-1)^l g(\cdot)$ is strictly increasing on the intervals $(l(l-1), l(l+1))$.*

Proof: We have

$$Z'(k) + (-1)^l g'(k) = 2k \sum_{j=0}^{\infty} \frac{2j+1}{(j(j+1) - E)^2} (1 + (-1)^{j+l}) > 0. \quad \blacksquare$$

Lemma 4.2 *We have*

$$g(k) = \frac{(-1)^l}{4\pi} \left(-\frac{2l-1}{l(l-1)-E} + \frac{2l+1}{l(l+1)-E} \right) + \mathcal{O}(1)$$

for $E \in (l(l-1), l(l+1))$ and any positive integer l with the error term independent of l . Moreover, there is a $K > 0$ such that $g(k) \geq K$ holds for all k large enough.

Proof: The error can be estimated explicitly; we shall show that

$$\left| g(k) - \frac{(-1)^l}{4\pi} \left(-\frac{2l-1}{l(l-1)-E} + \frac{2l+1}{l(l+1)-E} \right) \right| < \frac{1}{2\pi}. \quad (4.21)$$

To this end we have to find a bound to (4.18) on the interval $(l(l-1), l(l+1))$ with the two singular terms removed. The terms to the left and to the right of this pair form alternative sequences with the decreasing modulus, and as such each of them may be estimated by the (modulus of) the first term of such a sequence, *i.e.*, by

$$\frac{1}{4\pi} \left| \frac{2l-3}{(l-1)(l-2)-E} \right| \quad \text{and} \quad \frac{1}{4\pi} \left| \frac{2l+3}{(l+1)(l+2)-E} \right|,$$

respectively. Taking the maxima of these expressions and summing them we arrive at (4.21). To get the second claim, we have to compare this result with a lower bound to the modulus of the sum of the two singular terms. The minimum $\pi^{-1} + \mathcal{O}(l^{-1})$ of the latter is reached at $E = l^2 - \frac{1}{4} + \mathcal{O}(l^{-2})$, so this part wins over the other one once the error terms become small enough. ■

Lemma 4.3 *For a positive integer l and $E \in (l(l-1), l(l+1))$ we have*

$$Z(k) = \frac{1}{4\pi} \left(\frac{2l-1}{l(l-1)-E} + \frac{2l+1}{l(l+1)-E} \right) - \frac{\ln l}{2\pi} + \mathcal{O}(1), \quad (4.22)$$

where the error term is independent of l .

Proof: We again split the two singular terms in (4.22) and write the rest as $Z_-(k, l) + Z_+(k, l) - \frac{\ln l}{2\pi} + c(G)$, where

$$Z_-(k, l) := \frac{1}{4\pi} \sum_{j=1}^{l-2} \left(\frac{2j+1}{j(j+1)-E} - \sum_{n=0}^{2j} \frac{1}{j^2+n+1} \right),$$

$$Z_+(k, l) := \frac{1}{4\pi} \sum_{j=l+1}^{\infty} \left(\frac{2j+1}{j(j+1)-E} - \sum_{n=0}^{2j} \frac{1}{j^2+n+1} \right).$$

It is easy to see that

$$\sum_{n=0}^{2j} \frac{1}{j^2+n+1} = \frac{2}{j} + \mathcal{O}(j^{-2})$$

as $j \rightarrow \infty$, so the j -th term in $Z_{\pm}(k, l)$ can be estimated from above by

$$\frac{1}{4\pi} \left(\frac{2j+1}{j(j+1) - l(l+1)} - \frac{2}{j} + \mathcal{O}(j^{-2}) \right)$$

and from below by the same expression with $l(l+1)$ replaced by $l(l-1)$. Using the identity

$$\frac{2j+1}{j(j+1) - l(l+1)} = \frac{1}{j+l+1} - \frac{1}{l-j}$$

we find

$$\begin{aligned} 4\pi Z_-(k, l) &= \left(-\sum_{m=2}^{l-1} + \sum_{m=l+2}^{2l-1} - 2\sum_{m=1}^{l-2} \right) \frac{1}{m} + \sum_{m=1}^{l-2} \mathcal{O}(m^{-2}) = -3\ln l + \mathcal{O}(1), \\ 4\pi Z_+(k, l) &= \lim_{n \rightarrow \infty} \left[\left(\sum_{m=1}^{n-l} + \sum_{m=2l+2}^{n+l+1} - 2\sum_{m=l+1}^n \right) \frac{1}{m} + \sum_{m=l+1}^n \mathcal{O}(m^{-2}) \right] \\ &= \lim_{n \rightarrow \infty} \ln \frac{(n-l)((n+l+1))}{n^2} + \ln(l+1) + \mathcal{O}(1) = \ln l + \mathcal{O}(1). \end{aligned}$$

Summing the expressions we get the upper bound in (4.22); the lower one is obtained in the same way. \blacksquare

Lemma 4.4 *For any l large enough the interval $(l(l-1), l(l+1))$ contains a point μ_l such that $\Delta(\sqrt{\mu_l}) = 0$. The number μ_l has the following properties:*

- (i) $l(l+1) - \mu_l = 2l(\ln l)^{-1} (1 + \mathcal{O}(1))$,
- (ii) $\frac{2l+1}{l(l+1)-E} \leq \ln l + \mathcal{O}(1)$ for $E \leq \mu_l$,
- (iii) $\frac{2l-1}{l(l-1)-E} = \mathcal{O}(1)$ for $E > \mu_l$,
- (iv) finally, $\frac{Z(\sqrt{\mu_l})}{g(\sqrt{\mu_l})} = -1 + \mathcal{O}((\ln l)^{-1})$.

Proof: Fix l . We have $Z(k)^2 - g(k)^2 = (Z(k) + (-1)^l g(k))(Z(k) - (-1)^l g(k))$, and by the preceding lemmas these expressions equal

$$\frac{1}{2\pi} \frac{2l \pm 1}{l(l \pm 1) - E} - \frac{1}{2\pi} \ln \rho + \mathcal{O}(1).$$

The term with the minus sign is negative in $(l(l-1), l(l+1))$ provided l is large enough. The other term is sign changing for large l so it has a root. In view of Lemma 4.1 there is just one μ_l such that

$$\frac{2l+1}{l(l+1) - \mu_l} - \ln l + \mathcal{O}(1) = 0; \tag{4.23}$$

this proves (i). The relation (4.23) yields also the next two claims:

$$\frac{2l+1}{l(l+1)-E} \leq \frac{2l+1}{l(l+1)-\mu_l} = \ln l + \mathcal{O}(1) \quad (4.24)$$

and

$$\left| \frac{2l-1}{l(l-1)-E} \right| \leq \frac{2l-1}{\mu_l - l(l-1)} = \frac{2l-1}{2l \left(1 - \frac{1+\mathcal{O}(1)}{\ln l}\right)} = \mathcal{O}(1). \quad (4.25)$$

Finally, (iv) follows from (ii) and (iii) which yield

$$Z(\sqrt{\mu_l}) = \frac{1}{4\pi} (\ln l + \mathcal{O}(1)) - \frac{1}{2\pi} \ln l + \mathcal{O}(1) = -\frac{1}{4\pi} \ln l + \mathcal{O}(1)$$

and $|g(\sqrt{\mu_l})| = \frac{1}{4\pi} \ln l + \mathcal{O}(1)$. ■

Now we are in position to prove the main result of this subsection:

Theorem 4.5 *Let $K_\varepsilon := \mathbb{R} \setminus \bigcup_{l=2}^\infty (\mu_l - \varepsilon(l)(\ln l)^{-2}, \mu_l + \varepsilon(l)(\ln l)^{-2})$, where $\varepsilon(\cdot)$ is a positive strictly increasing function which tends to ∞ and obeys the inequality $|\varepsilon(x)| \leq x \ln x$ for $x > 1$. Then there is a positive c such that the transmission probability satisfies the bound*

$$|t(k)|^2 \leq c\varepsilon(l)^{-2} \quad (4.26)$$

for $k^2 \in K_\varepsilon \cap (l(l-1), l(l+1))$ and any l large enough. On the other hand, there are sharp resonance peaks localized on K_ε ,

$$|t(\sqrt{\mu_l})|^2 = 1 + \mathcal{O}((\ln l)^{-1}) \quad (4.27)$$

as $l \rightarrow \infty$.

Proof: In the first part we are going to estimate the modulus of the numerator in (4.20) from below. The leading term at high energies is the one with $\Delta(k)$; we shall estimate it on the set K_ε ; i.e., away of the zeros of the coefficient. Consider the neighborhood

$$I_l := (\mu_l - 2l(\ln l)^{-1}, \mu_l + 2l(\ln l)^{-1})$$

of μ_l on which the following estimates are valid:

$$\begin{aligned} \frac{1}{2k} \left(Z'(k) + (-1)^l g'(k) \right) &= \sum_{m=0}^{\infty} \frac{2m+1}{m(m+1)-E} \left(1 + (-1)^{l+m} \right) \\ &= \left(\sum_{m=0}^{l-2} + \sum_{m=l+1}^{\infty} \right) \frac{2m+1}{(m(m+1)-E)^2} (1 + (-1)^{l+m}) + \frac{2(2l+1)}{(l(l+1)-E)^2} \\ &\geq \frac{2(2l+1)}{(l(l+1)-E)^2} \geq \frac{2(2l+1)}{(l(l+1)-\mu_l+2l(\ln l)^{-1})^2} \\ &= \frac{2(2l+1)}{(2l(\ln l)^{-1}(2+\mathcal{O}(1)))^2} \geq c_1 \frac{(\ln l)^2}{l} \end{aligned}$$

for some $c_1 > 0$. Combining this result with Lemma 4.1 we are able to say how are the factors constituting $\Delta(k)$ separated from zero for $E \in (l(l-1), l(l+1))$ which does not belong to the interval $(\mu_l - \varepsilon(l)(\ln l)^{-2}, (\mu_l + \varepsilon(l)(\ln l)^{-2}) \subset I_l$:

$$\left| Z(k) + (-1)^l g(k) \right| \geq \varepsilon(l)(\ln l)^{-2} c_1 l^{-1} (\ln l)^2 = c_1 l^{-1} \varepsilon(l). \quad (4.28)$$

Now we begin estimating the modulus of the transmission amplitude from below. In the following, c_j always means a positive constant. Using the expression (4.20) we get a simple lower bound,

$$|t(k)| \leq \frac{4\pi\rho}{\left| \frac{1-2\pi Z(k)}{k|g(k)|} - \frac{\pi^2 \Delta(k)}{|g(k)|} (k^{-1} - 4k\rho^2) \right|}, \quad (4.29)$$

is obtained by neglecting the imaginary part of the denominator. First we shall show that

$$\frac{1 - 2\pi Z(E)}{k|g(k)|} = \mathcal{O}(1) \quad (4.30)$$

as $l \rightarrow \infty$. Using Lemmas 4.2 and 4.3 we estimate this expression by

$$\frac{|\ln l + \mathcal{O}(1)|}{kK} + \frac{1}{2\pi k} \left| \frac{\frac{2l+1}{l(l+1)-E} + \frac{2l-1}{l(l-1)-E}}{\frac{2l+1}{l(l+1)-E} - \frac{2l-1}{l(l-1)-E} - 2} \right| \leq c_2,$$

where in the second term we have used the explicit lower bound on $|g(k)|$, estimated the modulus of the fraction by $\frac{2l+1}{l-1} \leq 5$, and employed finally $k = \sqrt{E} = l + \mathcal{O}(1)$. For the second term in the denominator of (4.29) we shall show that

$$\frac{\pi^2 \Delta(k)}{|g(k)|} (k^{-1} - 4k\rho^2) \geq c_3 \varepsilon(l) \quad (4.31)$$

holds for all $E \in (l(l-1), l(l+1)) \setminus (\mu_l - \varepsilon(l)(\ln l)^{-2}, \mu_l + \varepsilon(l)(\ln l)^{-2})$, which will give (4.26) with $c := \left(\frac{c_3}{4\pi\rho}\right)^2$. Consider first the case $E \leq \mu_l$, when (4.28) together with Lemmas 4.4(ii) yield

$$\begin{aligned} & \pi^2 \left| k^{-1} - 4k\rho^2 \right| \frac{\left| Z(k) + (-1)^l g(k) \right| \left| Z(k) - (-1)^l g(k) \right|}{\left| \frac{1}{4\pi} \left(\frac{2l+1}{l(l+1)-E} - \frac{2l-1}{l(l-1)-E} \right) + \mathcal{O}(1) \right|} \\ & \geq 4\pi^2 \rho^2 k \left| 1 - (2\rho k)^{-2} \right| \frac{c_1 l^{-1} \varepsilon(l) \frac{1}{2\pi} \left| \frac{2l-1}{l(l-1)-E} - \ln l + \mathcal{O}(1) \right|}{\left| -\frac{1}{4\pi} \frac{2l-1}{l(l-1)-E} - \frac{1}{4\pi} \ln l + \mathcal{O}(1) \right|} \\ & \geq c_4 k \frac{\varepsilon(l)}{l} \geq c_5 \varepsilon(l), \end{aligned}$$

where in the last step we used again $k = l + \mathcal{O}(1)$. Let further $E > \mu_l$. We divide the argument into two parts. First we suppose

$$\frac{2l+1}{l(l+1)-E} \leq 2 \ln l;$$

then

$$\begin{aligned} \pi^2 \left| k^{-1} - 4k\rho^2 \right| & \frac{\left| Z(k) + (-1)^l g(k) \right| \left| Z(k) - (-1)^l g(k) \right|}{\left| \frac{1}{4\pi} \left(\frac{2l+1}{l(l+1)-E} - \frac{2l-1}{l(l-1)-E} \right) + \mathcal{O}(1) \right|} \\ & \geq 4\pi^2 \rho^2 k \left| 1 - (2\rho k)^{-2} \right| \frac{c_1 l^{-1} \varepsilon(l) \left| \ln l + \mathcal{O}(1) \right|}{\left| \ln l + \mathcal{O}(1) \right|} \geq c_6 \varepsilon(l) \end{aligned}$$

by (4.28) and Lemma 4.4(iii). On the other hand, if

$$\frac{2l+1}{l(l+1)-E} \geq 2 \ln l, \quad (4.32)$$

the same expression is bounded from below by

$$\begin{aligned} 4\pi^2 \rho^2 k \left| 1 - (2\rho k)^{-2} \right| & \frac{\left| \frac{1}{4\pi} \frac{2l+1}{l(l+1)-E} + \mathcal{O}(1) \right| \left| \frac{1}{2\pi} \ln l + \mathcal{O}(1) \right|}{\left| \frac{1}{4\pi} \frac{2l+1}{l(l+1)-E} + \mathcal{O}(1) \right|} \\ & \geq c_7 k \left| 1 - (2\rho k)^{-2} \right| \ln l \geq c_8 \varepsilon(l), \end{aligned}$$

where the denominator and the first term in the numerator have been estimated by means of (4.23) and (4.32), in the second term we have neglected one of the two terms of the same sign, and the last inequality follows from the fact that $x \ln x \geq \varepsilon(x)$ by assumption. To conclude the proof of (4.26), it is sufficient to put $c_3 := \min\{c_5, c_6, c_8\}$ in (4.31).

The rest is easier; the existence of resonance peaks at which the sphere is almost transparent follows from the relations

$$\begin{aligned} |t(\mu_l)| & = \left| \frac{1}{4\pi\rho\sqrt{\mu_l}g(\sqrt{\mu_l})} - \frac{Z(\sqrt{\mu_l})}{g(\sqrt{\mu_l})} \left(i + \frac{1}{2\rho\sqrt{\mu_l}} \right) \right|^{-1} \\ & = \left| \left(i + \frac{1}{2\rho\sqrt{\mu_l}} \right) (1 + \mathcal{O}((\ln l)^{-1})) + \frac{1}{\rho\sqrt{\mu_l}} (\ln l + \mathcal{O}(1)) \right|^{-1} \\ & = \left| i + \mathcal{O}((\ln l)^{-1}) \right|^{-1} = 1 + \mathcal{O}((\ln l)^{-1}), \end{aligned}$$

where we have used Lemma 4.4(iv). \blacksquare

4.4 A “bubble” array

Having proved this we illustrate the behavior by numerical results. We find interesting the behavior of $|t(k)|^2$. The curve oscillates almost regularly, but with the amplitude spanning from small values to unity for sufficiently large k . The lower enveloping curve of $|t(k)|^2$ behaves as $(E \ln E)^{-1}$ as we proved above. However, the behavior of $|t(k)|^2$ resembles that of δ^l -interaction, if an smoothed (locally averaged) curve is compared, as already mentioned above. This suspicion can be supported

by Fig. 7; it compares an averaged $|t(k)|^2$ of a “bubble” on the line and $|t(k)|^2$ of δ' -interaction. The averaging is done over ten neighboring peaks of a given point. The strength of the δ' -interaction is chosen so as to reach the same value of $|t(k)|^2$ at a distant k . These two curves seem to have the same “asymptotic” behavior.

Fig. 8 shows the band spectrum of an infinite array of bubbles on the line. What is different from analogical spectra of loop or comb arrays is the concentration of bands to small values ρ (note the logarithmic scale).

A A direct derivation of the comb-graph S-matrix

To illustrate the advantages of the formulas (2.31) and (2.32), we present two other ways to derive the comb-shaped graph S-matrix.

The first proof: By brute force, looking directly for the generalized eigenvector of H_N at the energy k^2 . One takes for the line component of the wavefunction the following Ansatz,

$$f(x) = \begin{cases} e^{ikx} + r_N e^{-ikx} & \dots & x < 0 \\ e_j e^{ikx} + f_j e^{-ikx} & \dots & L(j-1) < x < Lj \\ t_N e^{ikx} & \dots & x > L(N-1) \end{cases} \quad (\text{A.1})$$

for $j = 1, \dots, N-1$, while on the appendices we have multiples of the above specified solution to (3.6), $u_s = \beta_s u_\ell$, $s = 1, \dots, N$. We have to find the coefficients for which such a vector belongs *locally* to the domain of the Hamiltonian.

Substituting from (A.1) to (3.4) we get a system of linear equations; denoting

$$e_0 := 1, \quad f_n := 0, \quad e_N := t_N, \quad f_0 := r_N, \quad (\text{A.2})$$

we can write it concisely as

$$e_j \varepsilon^j + f_j \varepsilon^{-j} - e_{j+1} \varepsilon^j - f_{j+1} \varepsilon^{-j} = 0, \quad (\text{A.3})$$

$$e_{j+1} b \varepsilon^j + f_{j+1} b \varepsilon^{-j} + \beta_{j+1} (c u'_\ell(0) - u_\ell(0)) = 0, \quad (\text{A.4})$$

$$(ik-d)\varepsilon^j e_{j+1} + (ik+d)\varepsilon^{-j} f_{j+1} + ik\varepsilon^j e_j + ik\varepsilon^{-j} f_j + \beta_{j+1} b u'_\ell(0) = 0 \quad (\text{A.5})$$

for $j = 0, \dots, N-1$. First we express e_j from (A.3): by induction we check the relation

$$e_j = 1 + f_0 + \left(\sum_{l=1}^{j-1} f_l \varepsilon^{-2(l-1)} \right) (\varepsilon^{-2} - 1) - f_j \varepsilon^{-2(j-1)}. \quad (\text{A.6})$$

Using (A.4) we exclude e_{j+1} from (A.5), which yields

$$(2ik-d)\varepsilon^{-j} f_j - d e_j \varepsilon^j - 2ik\varepsilon^{-j} f_{j+1} + \beta_{j+1} b u'_\ell(0) = 0. \quad (\text{A.7})$$

Next we exclude β_j from (A.4) and (A.7); substituting then for e_j from (A.6) we get

$$\begin{aligned} -f_1 G + f_0[G-F] &= F, \\ -G\varepsilon^{-j}f_{j+1} + [(\varepsilon^2-1) + G]\varepsilon^{-j}f_j - \varepsilon^j F(1-\varepsilon^2) \left(\sum_{l=1}^{j-1} f_l \varepsilon^{-2l} \right) - \varepsilon^j f_0 &= 0, \end{aligned} \quad (\text{A.8})$$

where $j = 1, \dots, N-1$ and F, G are the quantities defined above. The last system can be transformed in such a way that its matrix is tridiagonal; to this end we add the j -th equation to the $(j-1)$ -th one multiplied by ε . The resulting system has the following form,

$$\begin{aligned} -f_1 d(cu'_\ell - u_\ell)(0) + f_0[G-F] &= F, \\ -Gf_{j+1} + [(1 + \varepsilon^2)G + (\varepsilon^2-1)F]f_j - G\varepsilon^2 f_{j-1} &= 0, \end{aligned} \quad (\text{A.9})$$

where $j = 2, \dots, N-1$. In terms of β, z this can be rewritten as

$$\begin{aligned} f_0(1 + i\beta) - f_1 &= -i\beta, \\ \varepsilon^{-1}f_{j+1} - 2zf_j + \varepsilon f_{j-1} &= 0, \quad j = 1, \dots, N-2, \\ -2zf_{N-1} + \varepsilon f_{N-2} &= 0; \end{aligned} \quad (\text{A.10})$$

we have taken into account here that $f_N = 0$. Now it is straightforward to find $f_0 = r_N$ as a ratio of the corresponding determinants, $r_N = D_N^{(2)}/D_N^{(1)}$, with

$$D_N^1 = -i\beta D_{N-1}, \quad D_N^2 = (1+i\beta)D_{N-1} + \varepsilon D_{N-2},$$

where

$$D_N := \begin{vmatrix} -2z & \varepsilon^{-1} & \dots & 0 & 0 \\ \varepsilon & -2z & \varepsilon^{-1} & \dots & 0 \\ \vdots & \vdots & \vdots & \vdots & \vdots \\ 0 & \dots & \varepsilon & -2z & \varepsilon^{-1} \\ 0 & 0 & \dots & \varepsilon & -2z \end{vmatrix}$$

and $D_0 := 0$. The above determinants satisfy the recursive relation $D_{N+2} + 2zD_{N+1} + D_N = 0$, so by induction we get $D_N = (-1)^N U_N(z)$, *i.e.*, the first formula in (3.8).

In a similar way we find the transmission amplitude. We start again from (A.3) from which we express f_j ,

$$f_j = \sum_{l=j}^{N-1} \varepsilon^{2l} (e_{l+1} - e_l), \quad j = 0, \dots, N-1.$$

Transforming the system we arrive at an analogy of (A.10) in the variables e_j ,

$$\begin{aligned} -2ze_1 + \varepsilon e_2 &= -\varepsilon^{-1}, \\ \varepsilon e_{j+2} - 2ze f_{j+1} + \varepsilon^{-1} e_j &= 0, \quad j = 1, \dots, N-2, \\ e_N(1 + i\beta) - e_{N-1} &= 0, \end{aligned}$$

which has to be solved for $e_N = t_N$. A disadvantage of this argument is that it gives a little insight into the way in which graph appendices contribute to the S-matrix.

The second proof: By S-matrix factorization described in Section 2.2. The on-shell S-matrix of a single tooth attached at $x = \xi$ is

$$S = \begin{pmatrix} e^{2ik\xi r} & t \\ t & e^{-2ik\xi r} \end{pmatrix}, \quad (\text{A.11})$$

where $t := t_1$ and $r := r_1$ are the corresponding amplitudes of a tooth attached at $x = 0$ which can be adopted from [25]. The matrix (A.11) is unitary since t/r is purely imaginary. The mentioned factorization technique yields for the amplitudes r_N and t_N the following recursive relations

$$r_{N+1} = r_N + \frac{\varepsilon^{2N} r t_N^2}{1 - \varepsilon^2 r r_N}, \quad t_{N+1} = \frac{t t_N}{1 - \varepsilon^2 r r_N}, \quad (\text{A.12})$$

which are equivalent to

$$t(r_{N+1} - r_N) = \varepsilon^{2N} r t_{N+1} t_N, \quad (1 - \varepsilon^2 r r_N) t_{N+1} = t t_N. \quad (\text{A.13})$$

Substituting from (3.8) into (A.13) and employing the relations between Chebyshev polynomials we check that r_N and t_N satisfy indeed (A.12). Certain disadvantage of this argument is that the closed form of the amplitudes (3.8) has to be guessed or derived by other means.

Acknowledgment

The research has been partially supported by GA AS under the contract # 1048801.

References

- [1] M.S. Abramowitz, I.A. Stegun, eds.: *Handbook of Mathematical Functions*, Dover, New York 1965.
- [2] V.M. Adamyan: Scattering matrices for microschemes, *Oper.Theory: Adv. Appl.* **59** (1992), 1–10.
- [3] R. Akis, P. Vasilopoulos, R. Debray: Ballistic transport in electron stub tuners: shape and temperature dependence, tuning of the conductance output, and resonant tunneling, *Ann. Phys.* **206** (1991), 440–492.
- [4] T. Aktosun, M. Klaus, C. van der Mee: On the number of bound states for the one-dimensional Schrödinger equation, *J. Math. Phys.* **39** (1998), 4249–4256.
- [5] S. Albeverio, F. Gesztesy, R. Høegh-Krohn, H. Holden: *Solvable Models in Quantum Mechanics*, Springer, Heidelberg 1988.
- [6] J. Asch, P. Duclos, P. Exner: Stability of driven systems with growing gaps. Quantum rings and Wannier ladders, *J. Stat. Phys.* **92** (1998), 1053–1069.

- [7] Y. Avishai, J.M. Luck: Quantum percolation and ballistic conductance on a lattice of wires, *Phys. Rev.* **B45** (1992), 1074–1095.
- [8] J.E. Avron, L. Sadun: Adiabatic quantum transport in networks with macroscopic components, *Ann. Phys.* **206** (1991), 440–492.
- [9] J.E. Avron, P. Exner, Y. Last: Periodic Schrödinger operators with large gaps and Wannier–Stark ladders, *Phys. Rev. Lett.* **72** (1994), 896–899.
- [10] J.E. Avron, A. Raveh, B. Zur: Adiabatic transport in multiply connected systems, *Rev. Mod. Phys.* **60** (1988), 873–915.
- [11] F. Barra, P. Gaspard: Scattering in periodic systems: from resonances to band structure, *J. Phys.* **A32** (1999), 3357–3375.
- [12] S.J. Blundell: The Dirac comb and the Kronig–Penney model: comment on [29], *Am. J. Phys.* **61** (1993), 1147–1148.
- [13] M. Büttiker: Small normal–metal loop coupled to an electron reservoir, *Phys. Rev.* **B32** (1985), 1846–1849.
- [14] L. Chico, V.H. Crespi, L.X. Benedict, S.G. Louie, M.L. Cohen: Pure carbon nanoscale devices: nanotube heterojunctions, *Phys. Rev. Lett.* **76** (1996), 971–974.
- [15] P. Exner: Lattice Kronig–Penney models, *Phys. Rev. Lett.* **74** (1995), 3503–3506.
- [16] P. Exner: Contact interactions on graph superlattices, *J. Phys.* **A29** (1996), 87–102.
- [17] P. Exner: Weakly coupled states on branching graphs, *Lett. Math. Phys.* **38** (1996), 313–320.
- [18] P. Exner: A duality between Schrödinger operators on graphs and certain Jacobi matrices, *Ann. Inst. H. Poincaré* **66** (1997), 359–371.
- [19] P. Exner: The absence of the absolutely continuous spectrum for δ' Wannier–Stark ladders, *J. Math. Phys.* **36** (1995), 4561–4570.
- [20] P. Exner, R. Gawlista: Band spectra of rectangular graph superlattices, *Phys. Rev.* **B53** (1996), 7275–7286.
- [21] P. Exner, P. Šeba: Quantum motion on a halfline connected to a plane, *J. Math. Phys.* **28** (1987), 386–381, 2254.
- [22] P. Exner, P. Šeba: Free quantum motion on a branching graph, *Rep. Math. Phys.* **28** (1989), 7–26.
- [23] P. Exner, P. Šeba: Resonance statistics in a microwave cavity with a thin antenna, *Phys. Lett.* **A228** (1997), 146–150.
- [24] P. Exner, P. Šeba, P. Šťovíček: Quantum interference on graphs controlled by an external electric field, *J. Phys.* **A21** (1988), 4009–4019.
- [25] P. Exner, P. Šerešová: Appendix resonances on a simple graph, *J. Phys.* **A27** (1994), 8269–8278.
- [26] P. Exner, M. Tater: Evanescent modes in multiple scattering factorization, *Czech. J. Phys.* **48** (1998), 617–624.
- [27] N.I. Gerasimenko, B.S. Pavlov: Scattering problem on noncompact graphs, *Teor. Mat. Fiz.* **74** (1988), 345–359 (in Russian).

- [28] J. Gratus, C.J. Lambert, S.J. Robinson, R.W. Tucker: Quantum mechanics on graphs, *J. Phys.* **A27** (1994), 6881–6892.
- [29] D.J. Griffith, N.F. Taussig: Scattering from a locally periodic potential, *Am. J. Phys.* **60** (1992), 883–888.
- [30] N. Hamada, S. Sawada, A. Oshiyama: New one–dimensional conductors: graphitic microtubules, *Phys. Rev. Lett.* **68** (1992), 1579–1581.
- [31] A.M. Jaynnavar, P. Singha Deo: Persistent current and conductance of metal loop connected to electron reservoir, *Phys. Rev.* **B49** (1994), 13685–13690.
- [32] A. Kasumov et al.: Conductivity and atomic structure of isolated multi-walled carbon nanotubes, *cond-mat/9710331*
- [33] A. Kiselev: Some examples in one–dimensional “geometric” scattering on manifolds, *J. Math. Anal. Appl.* **212** (1997), 263–280.
- [34] V. Kostykin, R. Schrader: Kirchhoff’s rule for quantum wires, *J. Phys.* **A32** (1999), 595–630.
- [35] V. Kostykin, R. Schrader: The generalized star product and the factorization of scattering matrices on graphs, *math-ph/0008022*.
- [36] P. Kuchment, Hongbiao Zeng: Convergence of spectra of mesoscopic systems collapsing onto a graph, mp_arc 00-308.
- [37] W. Porod, Zhi–An Shao, C.S. Lent: Transmission resonances and zeros in quantum waveguides with resonantly coupled cavities, *Appl. Phys. Lett.* **61** (1992), 1350–1352.
- [38] M. Reed, B. Simon: *Methods of Modern Mathematical Physics, IV. Analysis of Operators*, Academic Press, New York 1978.
- [39] M.G. Rozman, P. Reineker, R. Tehver: One–dimensional scattering: Recurrence relations and differential equations for transmission and reflection amplitudes, *Phys. Rev.* **A49** (1994), 3310–3321.
- [40] K. Ruedenberg, C.W. Scherr: Free–electron network model for conjugated systems, I. Theory, *J. Chem. Phys.* **21** (1953), 1565–1581.
- [41] M. Sassoli de Bianchi, M. Di Ventura: On the number of states bound by one–dimensional finite periodic potential, *J. Math. Phys.* **36** (1995), 1753–1764.
- [42] P. Singha Deo, A.M. Jaynnavar: Quantum waveguide transport in serial stub and loop structures, *Phys. Rev.* **B50** (1994), 11629–11639.
- [43] F. Sols, M. Macucci, U. Ravaioli, K. Hess: On the possibility of transistor action based on quantum interference phenomena, *Appl. Phys. Lett.* **54** (1989), 350–352.
- [44] F. Sols, M. Macucci, U. Ravaioli, K. Hess: Theory of quantum modulated transistor action, *J. Appl. Phys.* **66** (1989), 3892–3896.
- [45] D.W.. Sprung, Hua Wu, J. Martorell: Scatteing by a finite periodic potential, *Am. J. Phys.* **61** (1993), 1118–1124.
- [46] D. Takai, K. Ohta: Quantum oscillation in a multiply connected normal–conductor loop, *Phys. Rev.* **B50** (1994), 18250–18257.

- [47] E. Tekman, P.E. Bagwell: Fano resonances in quasi-one-dimensional quantum waveguides, *Phys. Rev.* **B48** (1993), 2553–2559.
- [48] K. Vacek, A. Okiji, H. Kasai: Ballistic transport in quantum wires with periodic bend structure, *Solid State Commun.* **85** (1993), 507–520.
- [49] Hongqui Xu: Scattering matrix method for ballistic electron transport: theory and application to quantum antidot arrays, *Phys. Rev.* **B50** (1994), 8469–8478.

Figure captions

Figures 2, 5, 8 available upon request from *tater@ujf.cas.cz*

Figure 1 A loop-graph scatterer in a magnetic field

Figure 2 The relation of transmission probabilities of a finite array of loops ($N = 6$) and the spectrum of the corresponding infinite system, $L_1 = 0.5$, $L_2 = 1.5$, $\ell = \sqrt{2}$, $\alpha_1 = -1$, $\alpha_2 = -2$.

Figure 3 A comb-shaped graph

Figure 4 The relation of transmission probabilities of a single appendix (dotted line), a finite array of appendices ($N = 7$) (full line), and the spectrum of the corresponding infinite system (thick lines above). The parameters are $b = 1.2$, $c = 0.5$, $d = 0$, $L = 1$, and $\ell = 1$.

Figure 5 The band spectra of infinite arrays of appendices. The upper figure is for $b = 1$, $c = d = 0$, and the lower one for $b = 3$, $c = 0.5$, and $d = -11$. The spacing is chosen $\ell = 1$ in both cases. The full lines show the role of perfect transmission (the lines in the bands) and total reflection (the lines in the gaps) for a single appendix.

Figure 6 This figure shows positions of resonances for $N = 5$ appendices and $b = 0.4$, $c = d = 0$, and $L = 1.2$. The dotted line separates the two sets of resonances. The resonances closer to the real axis have their origin in N -fold eigenvalue for $b = 0$; increasing $|b|$ lifts the degeneracy and pushes the resonances from the real line. The rest of the resonances (below the dotted line) has the origin in the serial arrangement of individual scatterers.

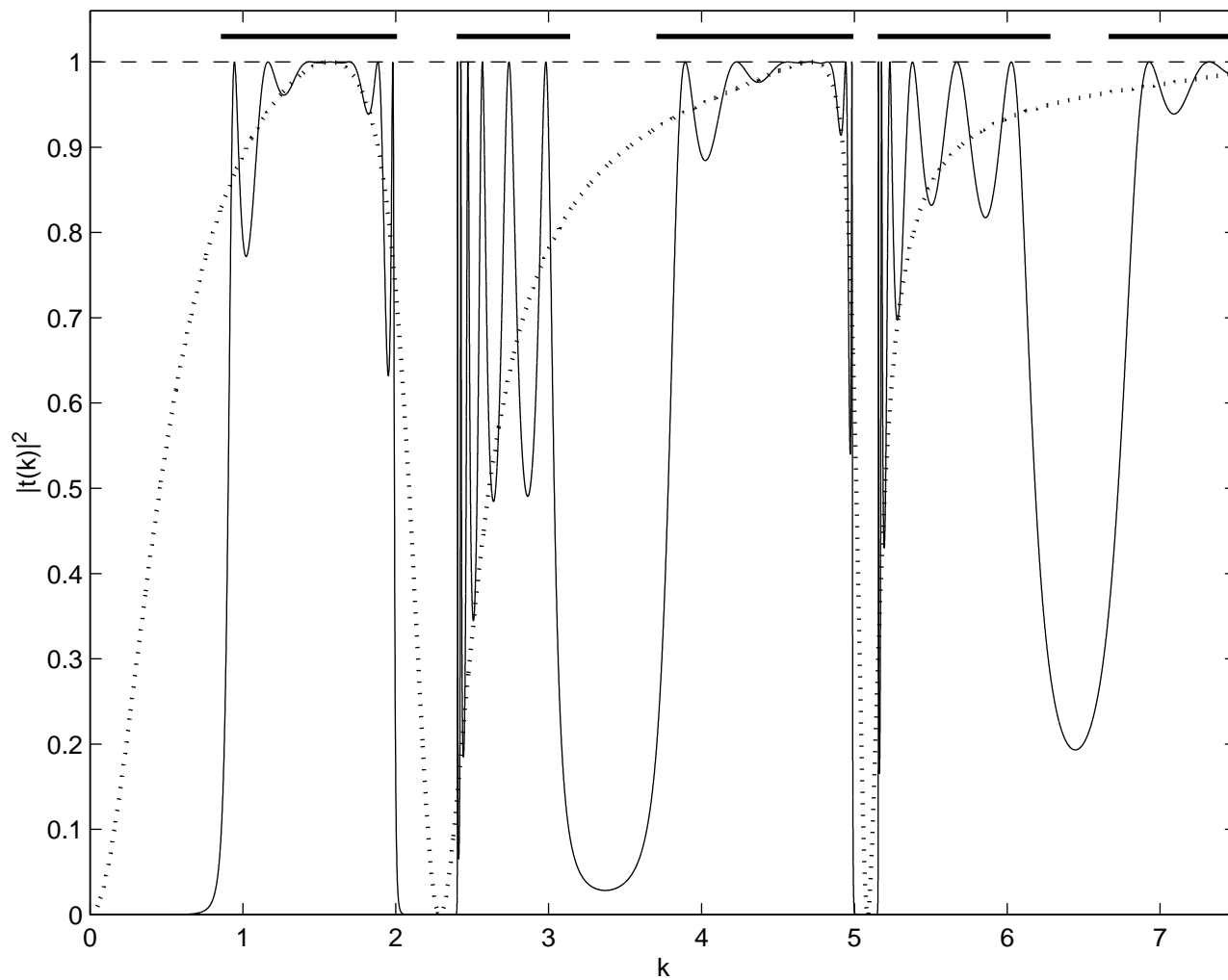
Figure 7 The transition probability of a sphere of unit radius on a line ($\rho = 0.01$). The lower graph compares the asymptotic behavior of $|t(k)|^2$ for δ' -interaction with suitably chosen strength and that of averaged transmission probability plotted in the upper graph. The averaging is done over ten neighboring peaks of each point.

Figure 8 Band spectrum of an infinite “bubble” array. The spheres are of unit radius, the spacing is $\ell = 1$ (upper figure) and $\ell = 0.01$ (lower figure), ρ is the contact radius.

This figure "figg2.jpeg" is available in "jpeg" format from:

<http://arxiv.org/ps/quant-ph/0103094v1>

Figure 4



This figure "figg5.jpeg" is available in "jpeg" format from:

<http://arxiv.org/ps/quant-ph/0103094v1>

Figure 6

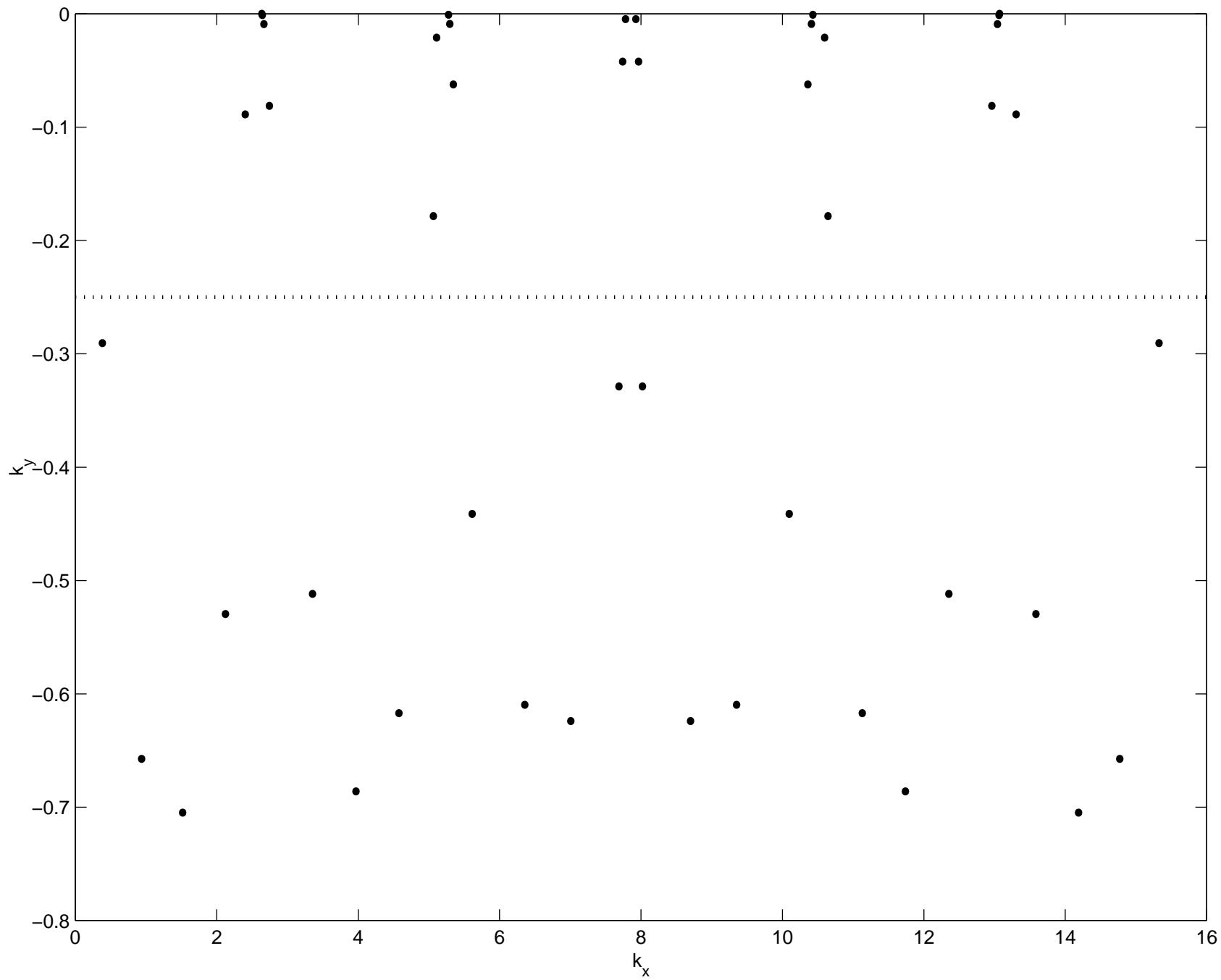
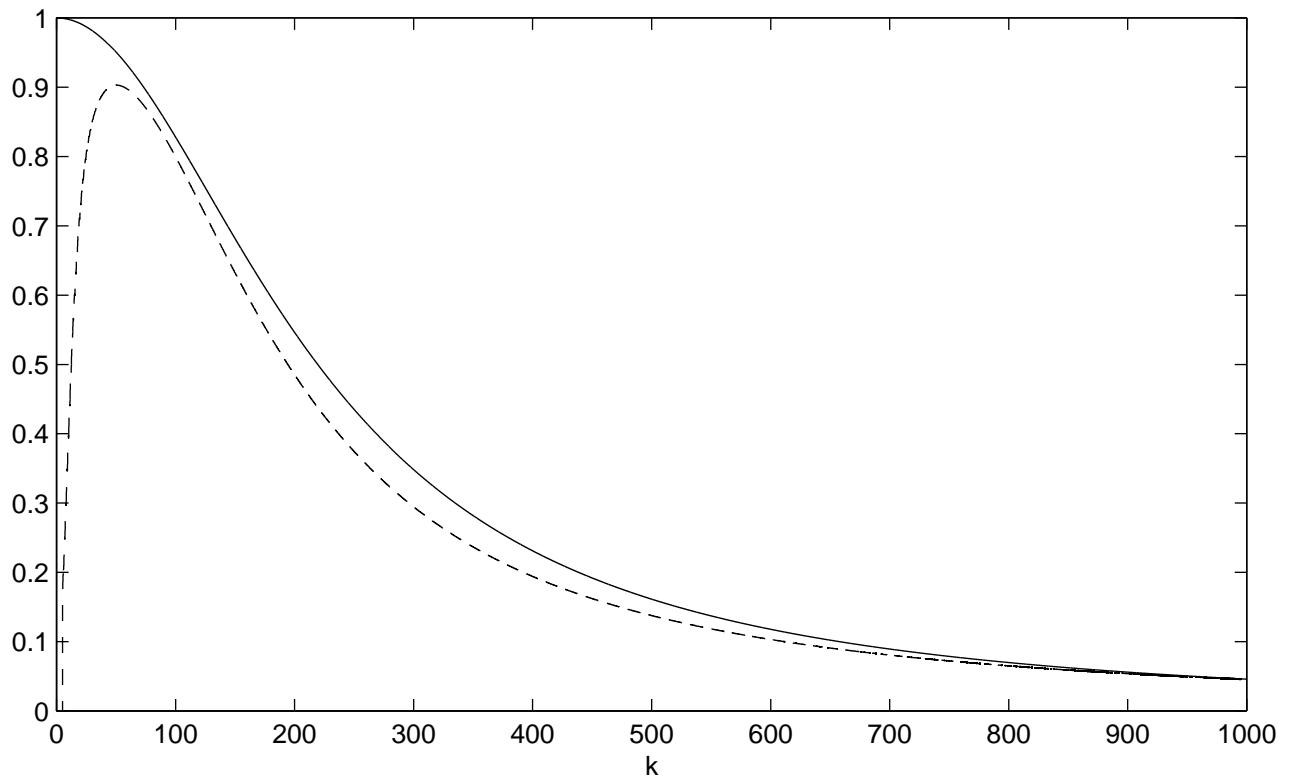
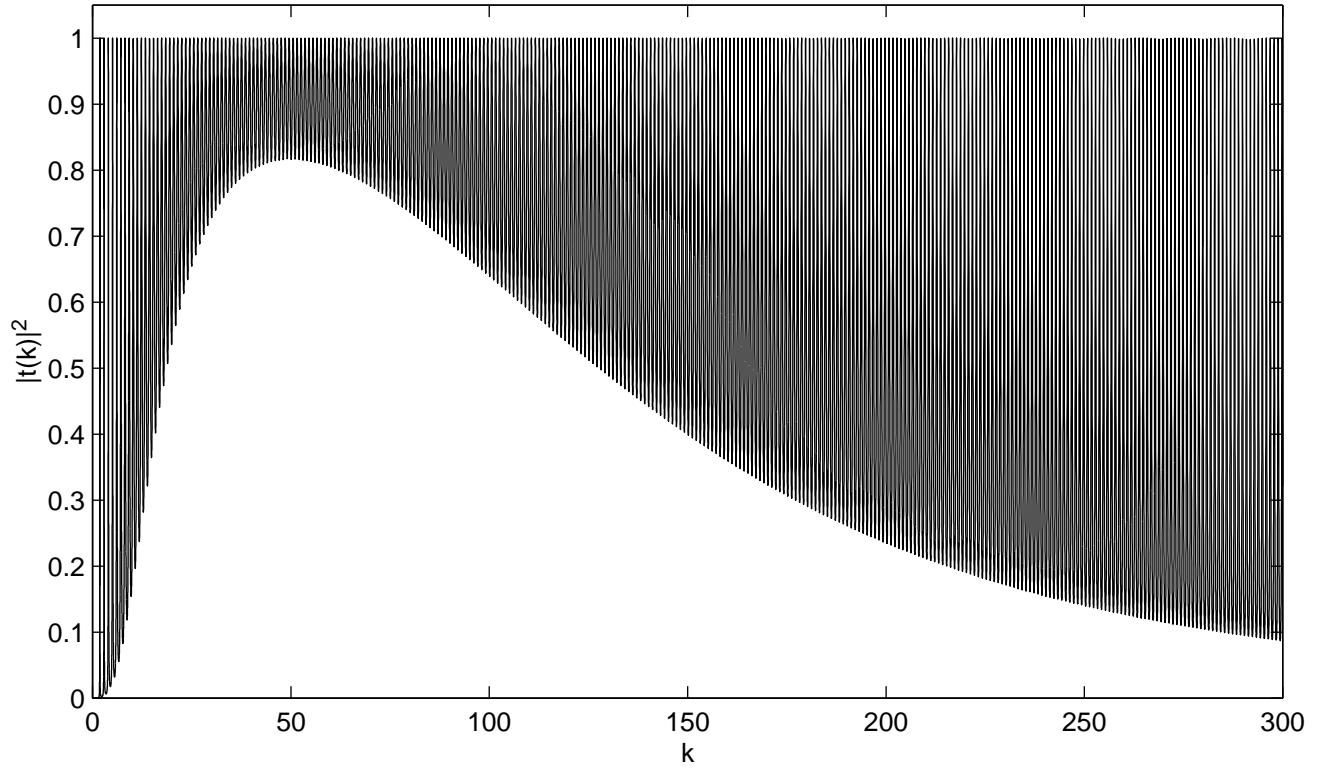


Figure 7



This figure "figg8.jpeg" is available in "jpeg" format from:

<http://arxiv.org/ps/quant-ph/0103094v1>